

UniBiomed: A Universal Foundation Model for Grounded Biomedical Image Interpretation

Linshan Wu¹, Yuxiang Nie¹, Sunan He¹, Jiaxin Zhuang¹,
Luyang Luo^{1,2}, Neeraj Mahboobani³, Varut Vardhanabhuti⁴,
Ronald Cheong Kin Chan^{5,6}, Yifan Peng⁷, Pranav Rajpurkar²,
Hao Chen^{1,8,9,10,11*}

¹Department of Computer Science and Engineering, The Hong Kong
University of Science and Technology, Hong Kong, China.

²Department of Biomedical Informatics, Harvard University, Boston,
USA.

³Department of Imaging and Interventional Radiology, The Chinese
University of Hong Kong, Hong Kong, China.

⁴Department of Diagnostic Radiology, Li Ka Shing Faculty of Medicine,
The University of Hong Kong, Hong Kong, China.

⁵Department of Anatomical and Cellular Pathology, The Chinese
University of Hong Kong, Hong Kong, China.

⁶State Key Laboratory of Translational Oncology, The Chinese
University of Hong Kong, Hong Kong, China.

⁷Population Health Sciences, Weill Cornell Medicine, New York, USA.

⁸Department of Chemical and Biological Engineering, The Hong Kong
University of Science and Technology, Hong Kong, China.

⁹Division of Life Science, The Hong Kong University of Science and
Technology, Hong Kong, China.

¹⁰State Key Laboratory of Molecular Neuroscience, The Hong Kong
University of Science and Technology, Hong Kong, China.

¹¹Shenzhen-Hong Kong Collaborative Innovation Research Institute,
The Hong Kong University of Science and Technology, Shenzhen, China.

*Corresponding author(s). E-mail(s): jhc@cse.ust.hk;

Abstract

The integration of AI-assisted biomedical image analysis into clinical practice demands AI-generated findings that are not only accurate but also interpretable to clinicians. However, existing biomedical AI models generally lack the ability to simultaneously generate diagnostic findings and localize corresponding biomedical objects. This limitation makes it challenging for clinicians to correlate AI-generated findings with visual evidence (*e.g.*, tiny lesions) in images and interpret the results of AI models. To address this challenge, we introduce **UniBiomed**, the first universal foundation model for grounded biomedical image interpretation, which is capable of generating accurate diagnostic findings and simultaneously segmenting the corresponding biomedical targets. UniBiomed is based on a novel integration of Multi-modal Large Language Model and Segment Anything Model, which can effectively unify diverse biomedical tasks in universal training for advancing grounded interpretation. To develop UniBiomed, we curate a large-scale dataset comprising over 27 million triplets of images, region annotations, and text descriptions across ten biomedical imaging modalities. Extensive validation on 70 internal and 14 external datasets demonstrated the state-of-the-art performance of UniBiomed in diverse biomedical tasks, including image segmentation, disease recognition, region-aware diagnosis, vision question answering, and report generation. In summary, UniBiomed is a powerful and versatile biomedical foundation model, unlocking the untapped grounded interpretation capability for optimizing AI-assisted biomedical image analysis.

Keywords: Biomedical Image Analysis, Foundation Model, Multi-modal Large Language Model, Universal Grounded Interpretation

1 Introduction

Multi-modal interpretation of biomedical images opens up novel opportunities in biomedical image analysis [1, 2]. Visual information from biomedical imaging enables detailed anatomical and functional analysis from cell to organ levels [3–7], while the textual information from diagnostic findings provides fine-grained descriptions for interpreting imaging [8–10]. However, it remains challenging for existing biomedical AI models to effectively integrate holistic vision and language information to assist clinicians in clinical practice. Although recent multi-modal biomedical foundation models [5, 8, 11, 12] have showcased encouraging results in interpreting biomedical images and generating diagnostic findings, these models are typically region-agnostic [13–15] and fail to extract the target regions (*e.g.*, tiny lesions) described in the generated findings. This limitation poses a critical barrier for clinicians to associate AI-derived findings with specific regions in images and interpret the results, significantly hindering the clinical practice of biomedical AI models.

Biomedical image segmentation is a practical solution for extracting structured visual information from biomedical images [3, 4, 6, 16–22], which enables the identification of regions of interest (ROI) across multiple scales, such as organs, lesions, tissues, and cells. Although recent segmentation foundation models [4, 16, 23, 24]

have demonstrated remarkable performance in this task, they generally lack the ability to generate diagnostic findings (*e.g.*, clinical reports), limiting their practicality in AI-assisted biomedical image analysis.

To address these challenges, we highlight the importance of grounded interpretation in biomedical image analysis, *i.e.*, generating diagnostic findings and simultaneously segmenting the corresponding biomedical targets. In this way, we enable biomedical AI models to deliver both accurate and interpretable results for effectively assisting clinicians in biomedical image analysis. In this work, we introduce **UniBiomed**, the first universal foundation model for grounded biomedical image interpretation. UniBiomed innovatively integrates advanced Multi-modal Large Language Models (MLLMs) [25, 26] and Segment Anything Model [27, 28] (SAM) for grounded biomedical image interpretation, as shown in **Figure 1 (c)**. Specifically, the MLLM is used to interpret multi-modal biomedical images and generate diagnostic findings. Then, we combine the encoded user instructions and the outputs of MLLM to prompt the SAM model for segmenting the biomedical objects corresponding to the generated findings. Through this integration, UniBiomed can tackle a wide range of biomedical tasks, including biomedical image segmentation, disease recognition, region-aware diagnosis, vision question answering (VQA), and report generation, as shown in **Figure 1 (d)**. These advancements enable UniBiomed to simultaneously provide fine-grained visual and textual information for fine-grained biomedical image analysis.

The power of UniBiomed originates from its ability to leverage holistic multi-modal biomedical information in universal training. Concretely, previous biomedical models typically rely on disjoint training with independent datasets, *e.g.*, clinical report datasets for report generation training [8, 12, 15, 29], segmentation datasets for segmentation training [4, 16, 19]. In contrast, our UniBiomed is versatile in utilizing different types of biomedical datasets to improve the performance of biomedical image analysis complementarily. Within a universal training process, training with segmentation datasets enables UniBiomed to extract critical biomedical objects, region-aware diagnosis datasets enhance the region-aware ability, and VQA and report generation datasets improve the model’s capability to interpret clinicians’ instructions and produce accurate diagnostic findings. Integrating complementary multi-modal datasets for training, UniBiomed demonstrates more powerful and versatile abilities in biomedical image analysis.

To develop UniBiomed, as shown in **Figure 1 (a) and (b)**, we curate a large-scale dataset containing 27 million triplets of images, region annotations, and text descriptions spanning 10 biomedical imaging modalities. Region annotations include both segmentation masks and bounding boxes, providing detailed spatial localization information for the model to develop region-aware capabilities. The text descriptions are extracted from readily available clinical texts accompanying public datasets, encompassing biomedical definitions, diagnostic findings, medical knowledge, and clinical reports. To the best of our knowledge, this is the largest and most comprehensive dataset for biomedical grounded interpretation. By integrating comprehensive and multi-granular visual and textual biomedical information for training, UniBiomed unleashes the untapped grounded interpretation capability in biomedical image analysis and achieves superior performance across diverse biomedical tasks.

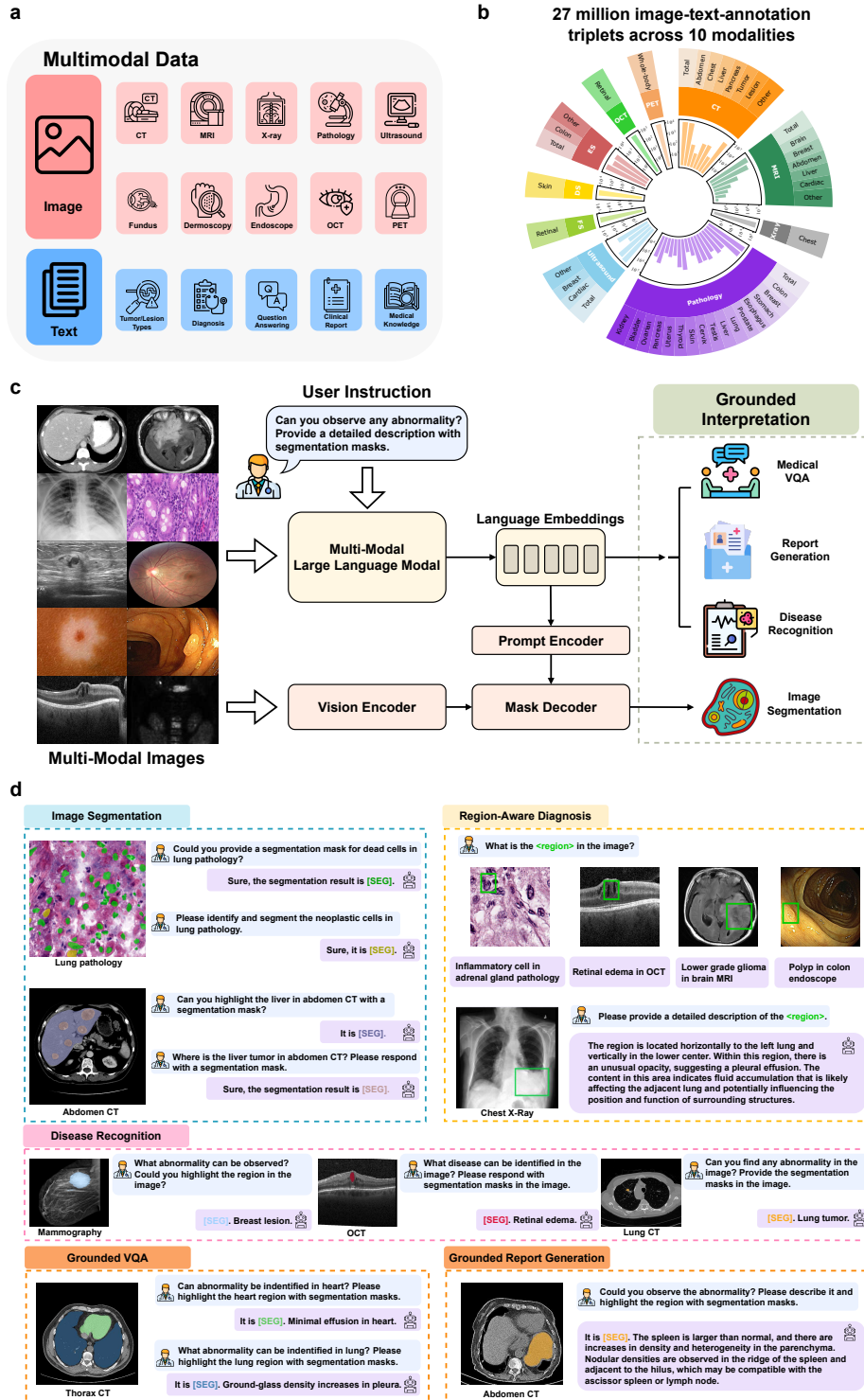


Fig. 1: Overview of the study. **a.** UniBiomed enables universal grounded interpretation across 10 different biomedical imaging modalities. CT, computed tomography; MRI, magnetic resonance imaging; OCT, optical coherence tomography; PET, positron emission tomography. **b.** We curated 27 million triplets of images, region annotations (segmentation masks and bounding boxes), and text descriptions for training UniBiomed. The text descriptions are processed from readily available diagnostic findings in public datasets. **c.** The framework of UniBiomed. UniBiomed incorporates Multi-modal Large Language Models (MLLMs) [25, 26] with Segment Anything Model [27, 28] (SAM) to tackle text description and segmentation tasks jointly. MLLM contains both vision and language models to interpret visual and language information, ultimately generating clinical text descriptions. SAM includes a vision encoder, a prompt encoder, and a mask decoder to address the segmentation task. Given user instructions with biomedical images, UniBiomed can segment target objects and generate grounded text descriptions simultaneously, enabling end-to-end analysis of multi-modal biomedical images. **d.** UniBiomed is designed to unify diverse biomedical tasks within a universal training process, including segmentation, disease recognition, region-aware diagnosis, vision question answering (VQA), and report generation.

We conduct a large-scale validation on 70 internal and 14 external datasets across 10 diverse biomedical imaging modalities. Extensive experiments demonstrate the effectiveness of UniBiomed. Specifically, in biomedical image segmentation, UniBiomed surpasses state-of-the-art segmentation foundation models [4, 16, 23, 24] by a substantial margin, *e.g.*, surpassing the representative model BiomedParse [4] by an average of 10.25% in Dice scores across 60 segmentation datasets. Beyond segmentation, UniBiomed also achieves superior performance in diverse biomedical tasks compared with state-of-the-art biomedical MLLMs, including disease recognition, VQA, ROI classification, region-aware report generation, and report generation. More importantly, we further showcase that UniBiomed is an effective biomedical AI tool for optimizing the biomedical image analysis workflow. Specifically, to recognize and localize abnormalities in images, previous biomedical AI models [4, 16, 23, 24] heavily rely on clinical experts to provide accurate textual or visual prompts, *e.g.*, instruct the model that the input image contains tumors (text prompts) or provide tight bounding boxes to highlight the tumors in the images (visual prompts). In contrast, UniBiomed can eliminate these processes and enable automated end-to-end grounded interpretation of biomedical images, effectively streamlining the analysis workflow. In summary, UniBiomed represents a versatile and powerful foundation model that delivers superior performance in grounded biomedical image interpretation, demonstrating promising potential towards more accurate and efficient biomedical image analysis.

2 Results

2.1 Overview of UniBiomed

Dataset. UniBiomed is designed to address the biomedical grounded interpretation tasks, necessitating training datasets to provide both region information and expert-annotated text descriptions. For the region information, we collect the readily available segmentation masks and bounding boxes from public biomedical datasets. Specifically, the segmentation masks are used for dense segmentation training. The bounding boxes are used for ROI classification and region-aware report generation training. Each of these segmentation masks and bounding boxes is paired with a specific text description, providing the biomedical classes or diagnostic findings of the annotated biomedical objects. To ensure high-quality text descriptions, we extract semantic labels, diagnostic findings, medical knowledge, and clinical reports from publicly available datasets following previous methods [4, 15, 29]. These descriptions capture fine-grained biomedical information across multiple granularities, including organs, lesions, tissues, and cells, enabling comprehensive interpretation of biomedical targets.

A critical step in our dataset pre-processing pipeline is transforming the textual descriptions into a uniform Vision-Question-Answering (VQA) format [12, 25, 30, 31], aiming to facilitate universal training. For example, given a CT image with liver tumors, we define the question as: *“Can you identify any abnormality within this CT image? Please respond with segmentation masks.”*. Then the corresponding answer is structured as: *“It is [SEG]. Liver tumor”*. For the ROI classification task without segmentation outputs, the answer will only contain the biomedical class without the *“[SEG]”* token [30, 31]. This uniform VQA format enables UniBiomed to jointly recognize abnormalities and segment biomedical targets within a universal foundation model. Some VQA examples are shown in **Extended Data Figure A3**.

Through this process, we construct a large-scale dataset consisting of **27 million** image-text-annotation triplets across 10 modalities, as shown in **Figure 1 (a) and (b)**. Specifically, the 3D medical images (CT and MRI) are pre-processed as 2D slices following previous methods [4, 16]. To the best of our knowledge, this is the largest and most comprehensive dataset for biomedical grounded interpretation. For example, compared with the dataset used in the representative biomedical foundation model BiomedParse [4], our dataset is over 30 times larger in scale. Unleashing the power of this large-scale dataset, UniBiomed demonstrates state-of-the-art performance across diverse tasks, outperforming existing biomedical foundation models [4, 12–14, 16, 23, 24] by a large margin. The details of the used datasets are presented in **Extended Data Tables A2, A3, A4, and A5**.

Method. Multi-modal Large Language Models (MLLMs) have achieved remarkable effectiveness in processing vision-language information [25, 32–35]. Typically, MLLMs leverage a vision encoder to encode images as vision tokens and input them into a Large Language Model (LLMs) [36] for text generation [25]. However, state-of-the-art MLLMs [25, 32–34] still fail to output the localizations of the corresponding regions described in the generated texts. This task, known as grounded interpretation in computer vision [30, 31, 37–40], requires a strong segmentation model to segment

the target regions. Segment Anything Model (SAM) [27, 28] has demonstrated promising results in segmenting diverse sources of images, including biomedical images [4, 16]. The advances in MLLMs [25, 32–34] and SAM [27, 28] lead to a promising way for us to investigate grounded biomedical image interpretation.

In this work, we introduce UniBiomed, which innovatively integrates MLLM [25, 26] and SAM [27, 28] for universal grounded interpretation of biomedical images. The overall framework is shown in **Figure 1 (c)**. Our approach combines the complementary strengths of MLLM and SAM: MLLM processes both visual and textual information to generate descriptive interpretations, while SAM performs precise image segmentation through its vision encoder, prompt encoder, and mask decoder modules.

The framework operates as an end-to-end way that, given user instructions and biomedical images, UniBiomed simultaneously: (1) generates text descriptions of the biomedical images, and (2) segments the corresponding biomedical targets. The effectiveness of UniBiomed arises from the complementary integration of MLLM and SAM. Specifically, UniBiomed combines the output of the last layer in the MLLM [30, 31, 41] with the tokenized user instructions as the language embeddings to guide SAM’s segmentation process. This incorporation effectively eliminates the manual efforts of crafting bounding boxes [16, 23] or detailed text descriptions [24, 42] as prompts for segmentation. For implementation, we select InternVL2.5 [26, 33] as our foundation MLLM due to its robust multi-modal understanding capabilities, and SAM2 [28] is adopted as our segmentation model for its improved segmentation performance. The details of the method are described in **Section 4.1**.

Evaluation. To demonstrate the effectiveness of UniBiomed on diverse biomedical tasks, we conduct a comprehensive evaluation on 70 internal and 14 external datasets. Since we focus on evaluating the effectiveness of grounded interpretation, for comparison methods, we compare segmentation foundation models [4, 16, 23, 24] on segmentation tasks, compare grounding tasks with grounding methods [31, 41], and compare medical MLLMs [12–14] on medical diagnosis tasks. **(1)** First, we conduct extensive comparisons with several foundation models [4, 16, 23, 24] in biomedical image segmentation. **(2)** Second, we evaluate UniBiomed in a challenging grounded VQA task, *i.e.*, grounded disease recognition, which aims to simultaneously generate diagnostic findings and segment the corresponding biomedical targets. **(3)** Then, we conduct extensive experiments on grounded report generation, which is designed to generate clinical reports of the given images and highlight the target regions. We verify the grounded report generation task on the RadGenome [29, 43] dataset. **(4)** Finally, we verify the effectiveness of UniBiomed in two region-aware diagnosis tasks: ROI classification and region-aware report generation. Specifically, we extract bounding boxes from segmentation masks to indicate the ROIs following previous methods [14, 44–46]. We assess the region-aware report generation task using the MedTrinity [15] dataset. The details of the datasets are presented in **Extended Data Tables A2, A3, A4, and A5**. More details of the evaluation are presented in **Section 4.3**.

2.2 UniBiomed excels in biomedical image segmentation

In this section, we present a comprehensive comparison with multiple biomedical segmentation foundation models in biomedical image segmentation, *i.e.*, MedSAM [16],

SegVol [23], SAT [24], and BiomedParse [4], as shown in **Figure 2**. Specifically, we evaluate our method on 46 internal and 14 external datasets across nine diverse biomedical imaging modalities. The details of the datasets are shown in **Extended Data Tables A2**. We adopt text prompts for referring segmentation as SAT [24] and BiomedParse [4]. For example, to segment liver tumors in CT, we provide a text instruction *“Please segment liver tumor in the CT image”* to the model, eliminating the need to offer visual prompts like bounding boxes or points as MedSAM [16] and SegVol [23]. More details of the competing methods are presented in **Section 4**.

As shown in **Figure 2 (a) and (b)**, UniBiomed achieves superior performance compared to state-of-the-art segmentation foundation models [4, 16, 23, 24]. Specifically, UniBiomed surpasses the best-competing method BiomedParse [4] by a clear margin, *i.e.*, 10.25% dice score improvements on 60 datasets across nine modalities. **Figure 2 (d)** shows that UniBiomed outperforms BiomedParse by 9.13% and 13.95% in 46 internal and 14 external datasets, respectively. These findings robustly underscore UniBiomed’s substantial advancement in universal biomedical image segmentation.

One of the key reasons for UniBiomed’s breakthrough in biomedical image segmentation lies in its ability to unleash the power of MLLM and SAM in large-scale multi-modal biomedical datasets. Unlike prior segmentation models [4, 16, 23, 24] that rely solely on segmentation datasets for training, UniBiomed effectively incorporates large-scale VQA and report generation datasets [15, 29] in universal training. This approach enables UniBiomed to develop more generalizable representations, leading to superior segmentation performance across diverse biomedical imaging modalities. As shown in **Figure 2 (e)**, with large-scale multi-modal datasets for training, we improve UniBiomed by 3.39% and 8.26% dice scores in internal and external validation, respectively.

More importantly, beyond segmentation, UniBiomed establishes a more comprehensive interpretation capability for biomedical image analysis, unlocking novel opportunities in broader clinical applications. As illustrated in **Figure 2 (f)**, prior segmentation models [4, 16, 23, 24] are still limited in tackling the segmentation tasks, which heavily hamper their clinical applications in biomedical image analysis. In contrast, UniBiomed extends segmentation to grounded interpretation with text generation, which is a versatile foundation model capable of handling diverse biomedical tasks, making it more adaptable for clinical applications.

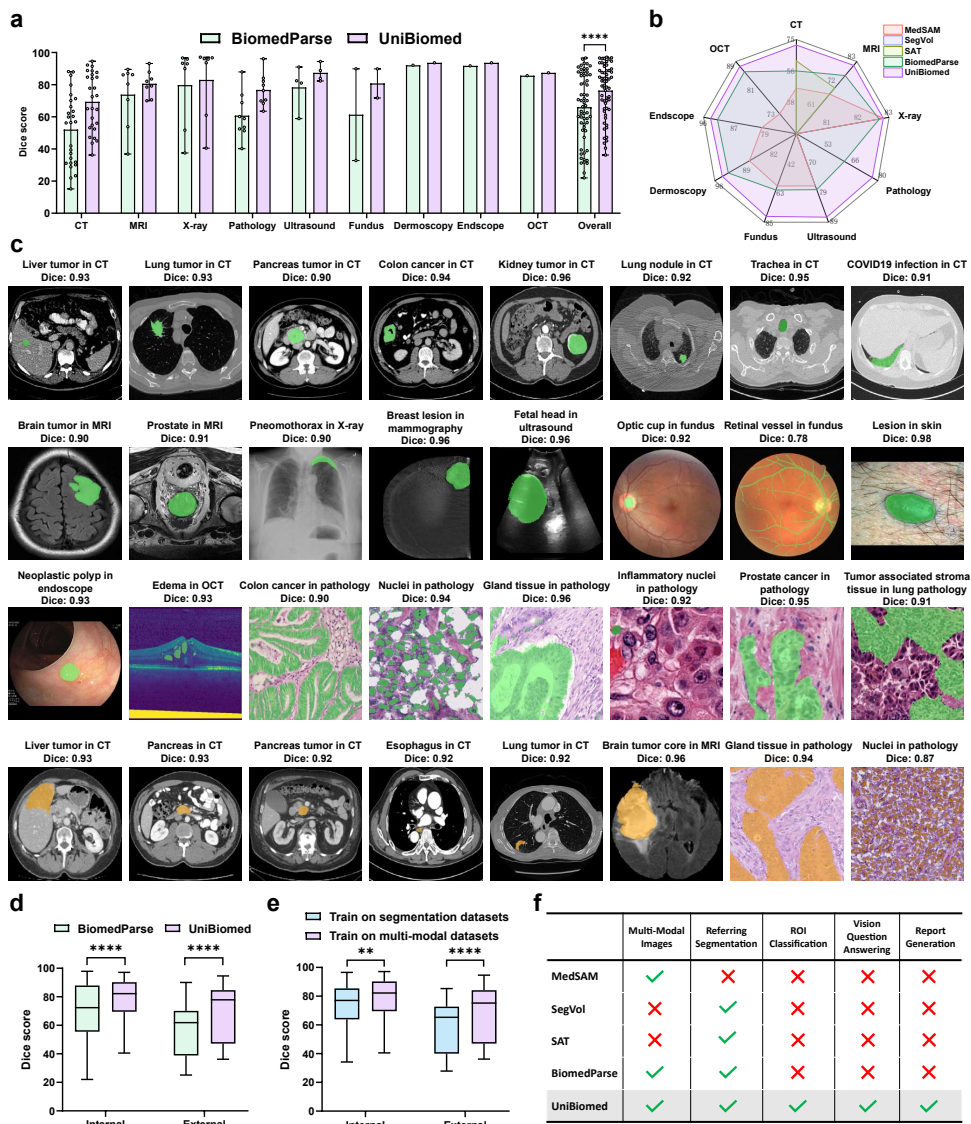


Fig. 2: Comparison of biomedical image segmentation. **a.** Comparison of Dice scores between UniBiomed and the best-competing segmentation foundation model BiomedParse [4] across nine modalities, with the mean (\pm s.d.) reported. Significance levels at which UniBiomed outperforms BiomedParse [4], with a two-sided paired t-test P -value of **** $P < 1 \times 10^{-4}$. Notably, UniBiomed outperforms BiomedParse [4] by an average of 10.25% in dice scores on 60 internal and external datasets. **b.** Radar chart comparisons with several representative segmentation foundation models, MedSAM [16], SegVol [23], SAT [24], and BiomedParse [4]. Specifically, SAT [24] is only applicable to 3D modalities like CT and MRI. SegVol [23] is solely available for CT datasets. **c.** Qualitative segmentation results of UniBiomed. Specifically, the colors of segmentation masks for internal and external validations are green and orange, respectively. **d.** Box plot comparisons between UniBiomed and BiomedParse [4]. Significance levels at which UniBiomed outperforms BiomedParse [4], with two-sided paired t-test P -values of **** $P < 1 \times 10^{-4}$ for both internal and external validations. **e.** Ablation studies of UniBiomed. We compare UniBiomed under two settings: (1) train on only segmentation datasets, and (2) train on large-scale multi-modal datasets, including segmentation, VQA, and report generation datasets. It can be seen that with large-scale multi-modal datasets for training, the segmentation performance can be further improved, the two-sided paired t-test P -values are ** $P < 1 \times 10^{-2}$ and **** $P < 1 \times 10^{-4}$ for internal and external validations, respectively. **f.** Overall application comparisons with representative biomedical segmentation models [4, 16, 23, 24]. Referring segmentation represents using text instructions as prompts for segmentation, which eliminates the efforts of providing tight bounding boxes for the biomedical objects [16]. Notably, UniBiomed not only supports multi-modal biomedical image segmentation but also establishes remarkable capabilities in ROI classification, VQA, and report generation, where state-of-the-art segmentation models [4, 16, 23, 24] fail to establish.

2.3 UniBiomed enables accurate grounded disease recognition

In medical MLLMs [8, 12, 29, 42, 47–49], disease recognition is one of the most important VQA tasks, which aims to identify the lesions, tumors, or abnormalities in the given images. However, existing medical MLLMs [8, 12, 29, 42, 47–49] are typically region-agnostic, which solely generate diagnostic findings but fail to localize relevant regions (*e.g.*, tiny lesions) in the images. This lack of spatial awareness severely limits their clinical applications, as precise localization of abnormalities is essential for diagnosis and treatment planning.

In this work, we introduce a novel and challenging grounded VQA task, *i.e.*, grounded disease recognition, which is designed to simultaneously generate diagnostic findings and segment the corresponding targets. In this task, the model is asked to predict abnormality class (*e.g.*, liver tumor or pancreas tumor) and segment the targets in the images. If there is no abnormality in the given images, the model is supposed to output “*No findings*” and produce all-zero segmentation masks.

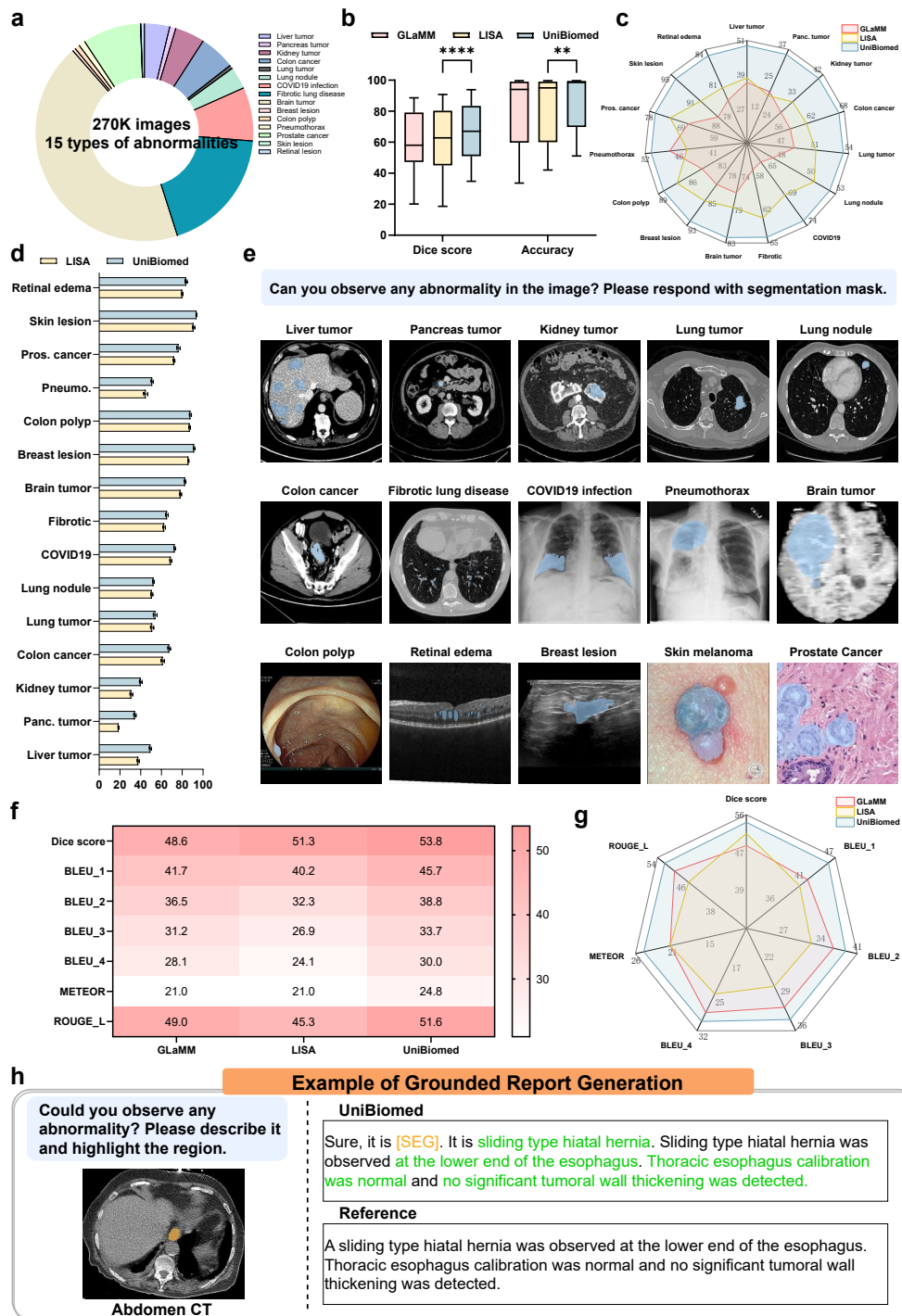


Fig. 3: Comparison of grounded disease recognition and grounded report generation. **a.** We curate a new dataset for grounded disease recognition. Specifically, this dataset contains 270K images with 15 types of abnormalities. The details of the dataset are presented in **Extended Data Table A6**. **b.** We compare UniBiomed with two state-of-the-art methods, LISA [31] and GLaMM [41], in segmentation dice scores and disease recognition accuracy. Notably, UniBiomed outperforms the best competing method LISA [31] by 3.86% in dice scores and 3.29% in accuracy, with two-sided paired t-test P -values of **** $P < 1 \times 10^{-4}$ and ** $P < 1 \times 10^{-2}$. **c.** Radar chart comparisons across 15 types of abnormalities. **d.** Dice scores comparisons between UniBiomed and LISA [31] across 15 types of abnormalities, with the mean (\pm s.d.) reported. **e.** The qualitative visualization results of grounded disease recognition. The template user instruction is shown in the blue box. Given template instructions, UniBiomed can recognize the abnormalities in the images and highlight the precise localizations. **f.** Comparisons of grounded report generation on the RadGenome [43] dataset. We re-implement GLaMM [41] and LISA [31] on this dataset for comparison. We report dice scores results for segmentation evaluation, BLEU [50], METEOR [51], and ROUGE-L [52] results for report generation evaluation. **g.** Radar chart comparisons across different metrics in grounded report generation. **h.** An example of grounded report generation on abdominal CT images. The template user instruction is shown in the blue box. The text in green indicates the correct contents. Reference denotes the ground truth from the RadGenome dataset [43]. The segmentation mask indicates the location of the corresponding organ (esophagus in the example) described in the report.

To this end, we curate a comprehensive dataset encompassing 15 distinct abnormality types for model training and validation, as shown in **Figure 3 (a)**. Specifically, these 15 abnormality types contain liver tumor, pancreas tumor, kidney tumor, colon cancer, lung tumor, lung nodule, COVID-19 infection, fibrotic lung disease, brain tumor, breast lesion, colon polyp, pneumothorax, prostate cancer, skin lesion, and retinal lesion. The details of the datasets are shown in **Extended Data Tables A2 and A6**.

Existing medical models lack the capability to tackle this task, which requires simultaneously outputting segmentation masks and diagnostic findings. Although BiomedParse [4] can conduct segmentation and employ a meta-object classifier for classification, this classifier requires users to pre-diagnose the images and provide diagnostic findings as textual prompts to the model, thus failing to perform the grounded disease recognition task introduced in this work. To this end, we re-implement two state-of-the-art approaches from the general domain, LISA [31] and GLaMM [41], on our curated datasets for fair comparisons. The comparison results are shown in **Figure 3 (b-d)**. Specifically, UniBiomed outperforms the best competing method LISA [31] by 3.86% and 3.29% in segmentation dice scores and disease recognition accuracy, respectively. Consistent improvements across different types of abnormalities are observed in **Figure 3 (d)**, which robustly validates the effectiveness of UniBiomed in this challenging VQA task.

More importantly, the strong capability of UniBiomed in grounded disease recognition potentially leads to a significant paradigm shift in the biomedical image analysis workflow. Specifically, previous biomedical foundation models heavily rely on clinical experts to pre-diagnose images and manually craft precise textual or visual prompts. For example, for the task of lung tumor recognition, one of the representative foundation models, MedSAM [16], requires radiologists to outline the regions of lung tumors in each slice of a 3D CT scan and provide the prompts to the model. Another representative foundation model, BiomedParse [4], necessitates radiologists to identify lung tumors in each slice of a 3D CT scan in advance, then input an instruction “Please segment lung tumor in this CT image” to prompt the model for lung tumor segmentation. In contrast, UniBiomed enables an end-to-end pipeline to recognize abnormalities in images. As shown in **Figure 3 (e)**, UniBiomed is free of pre-diagnosis by clinical experts. Instead, UniBiomed adopts a template instruction and automatically recognizes the abnormality class with segmentation predictions. These findings underscore the clinical practice of UniBiomed’s grounded interpretation capabilities, which is a non-trivial advancement compared to state-of-the-art biomedical foundation models [4, 16, 23, 24].

2.4 UniBiomed enables accurate grounded report generation

Grounded report generation is a challenging task that combines biomedical image segmentation with report generation, enabling end-to-end biomedical image analysis in a universal model. Unlike prior methods [4, 12–14], which rely on separate segmentation models and standalone language models for report generation, UniBiomed performs both tasks within one universal model. This integration allows UniBiomed to leverage holistic biomedical knowledge more effectively, improving both segmentation and report quality.

To evaluate its effectiveness, we conduct extensive comparisons on the RadGenome [43] dataset. Specifically, the RadGenome dataset is processed from the CT-RATE [29] dataset, which contains detailed CT reports with segmentation masks for training and validation. The clinical reports provide detailed descriptions of the images, and the segmentation masks indicate the localization of corresponding organs. Since existing medical MLLMs [8, 12–14, 42, 47–49] cannot tackle this task, we also re-implement GLaMM [41] and LISA [31] on our datasets for comparisons. The results are shown in **Figure 3 (f) and (g)**.

We report the dice scores results for segmentation evaluation, Bilingual Evaluation Understudy (BLEU) [50], Metric for Evaluation of Translation with Explicit Ordering (METEOR) [51], and Recall-Oriented Understudy for Gisting Evaluation (ROUGE_L) [52] results for report generation evaluation. The details of the evaluation metrics are described in **Section 4.3**. It can be observed that UniBiomed not only achieves better segmentation performance (53.8% dice scores) but also demonstrates superior report generation capabilities (45.7%, 24.8%, and 51.6% in BLEU₁, METEOR, and ROUGE_L, respectively). We further showcase an example of grounded report generation on abdomen CT images, as presented in **Figure 3 (h)**. Specifically, within an end-to-end process, UniBiomed can observe the “*sliding type hiatal hernia*” abnormality with detailed descriptions and highlight the anatomy

region of the esophagus with segmentation masks. In contrast, state-of-the-art methods [4, 8, 12–14, 16, 23, 24] require multiple models and stages to establish this diagnosis process, which is inflexible and inefficient in real-world deployment. More examples are presented in **Extended Data Figure A5**.

2.5 UniBiomed effectively improves region-aware diagnosis

Region-aware diagnosis refers to recognizing the biomedical objects within the user-defined ROIs in the images [14, 15]. We involve this task in our training to enhance the region-aware ability of UniBiomed and ultimately improve the performance of grounded interpretation. Following the settings of MedPLIB [14], we evaluate two region-aware diagnosis tasks in this work, *i.e.*, ROI classification and region-aware report generation. Since the segmentation predictions are not required in this task, we output the results by the MLLM module only. Following previous methods [15, 45], to indicate the ROIs, we directly overlay bounding boxes onto the images, eliminating the need for complex region encodings for indicating ROIs. The details are presented in **Section 4**.

We first evaluate the performance of ROI classification. For fair comparisons, we compare UniBiomed with two state-of-the-art medical MLLMs, MedRegA [13] and MedPLIB [14], since both of them were trained on large-scale ROI classification datasets. The results are shown in **Figure 4 (a-d)**. Specifically, UniBiomed achieves an average 93.38% accuracy in ROI classification, surpassing the best competing method MedPLIB [14] by an average of 8.32% in ROI classification accuracy across ten imaging modalities. These results validate that UniBiomed also excels in ROI classification compared with state-of-the-art methods.

We further evaluate a more challenging region-aware diagnosis task, *i.e.*, region-aware report generation, which aims to generate detailed reports within ROIs in the biomedical images. Our experiments are conducted on the MedTrinity [15] dataset, a large-scale benchmark featuring region-centric reports across diverse biomedical imaging modalities. Specifically, MedTrinity is aggregated from 23 public VQA and report generation datasets across 10 biomedical imaging modalities, as described in **Extended Data Table A3**. We compare our approach with several state-of-the-art MLLMs, including InternVL2.5 [26, 33], LLaVA-Med [12], MedRegA [13], and MedPLIB [14]. Among them, InternVL2.5 is the state-of-the-art MLLM in the general domain. LLaVA-Med, MedRegA, and MedPLIB are generalist MLLMs in the medical domain, while MedRegA and MedPLIB were trained on large-scale region-centric report generation datasets. We report the results of BLEU [50], METEOR [51], and ROUGE_L [52]. The details of the comparison methods are described in **Section 4.3**.

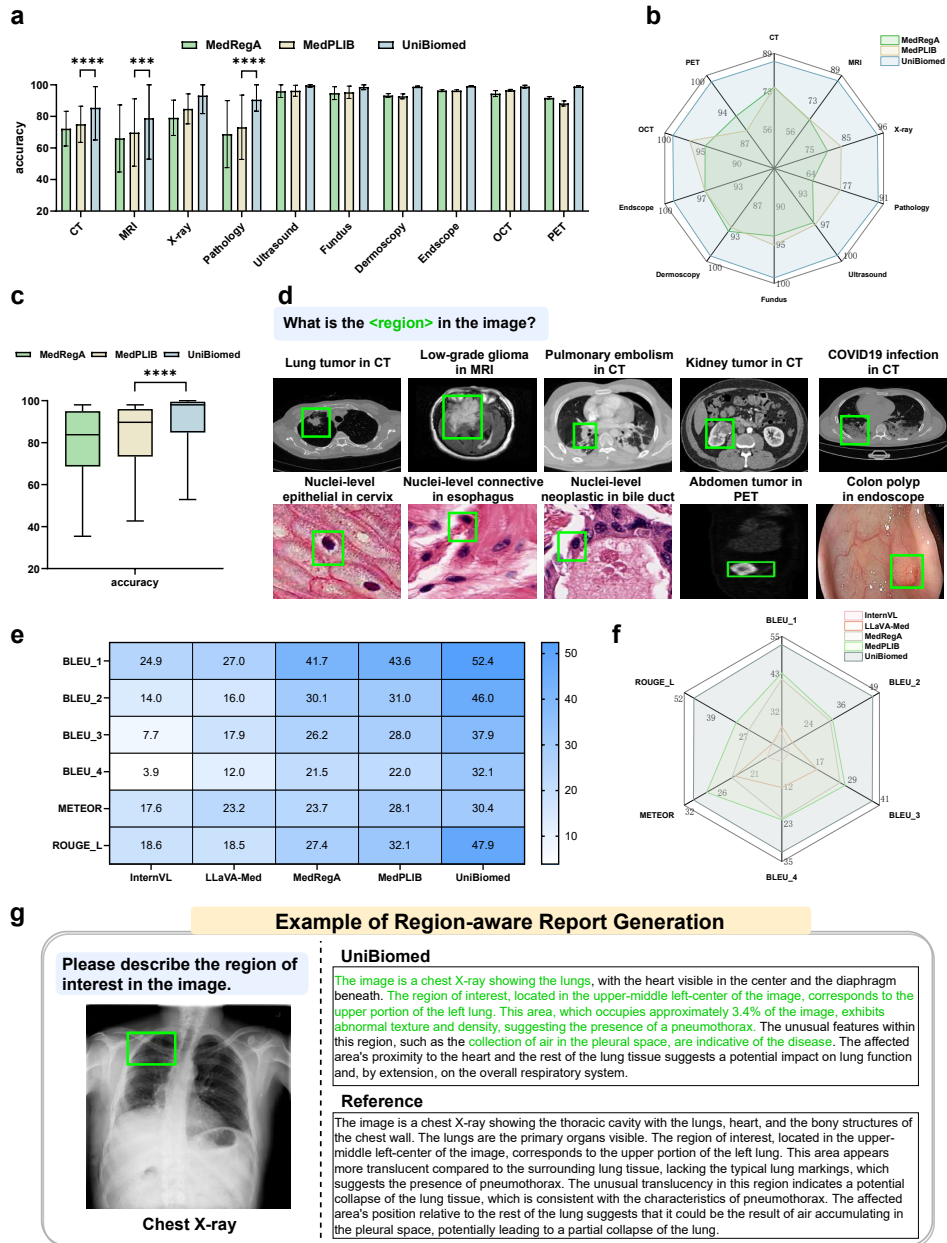


Fig. 4: Comparison of ROI classification and region-aware report generation. **a.** Comparisons with MedRegA [13] and MedPLIB [14] in ROI classification, with the mean accuracy (\pm s.d.) reported. Significance levels at which UniBiomed outperforms MedPLIB [14], with two-sided paired t-test P -values are **** $P < 1 \times 10^{-4}$, *** $P < 1 \times 10^{-3}$, and **** $P < 1 \times 10^{-4}$ for CT, MRI, and pathology, respectively. **b.** Radar chart comparison with MedRegA [13] and MedPLIB [14] across ten diverse biomedical imaging modalities. **c.** UniBiomed surpasses MedPLIB [14] by 8.32% in ROI classification accuracy, with two-sided paired t-test P -values of **** $P < 1 \times 10^{-4}$. **d.** Qualitative visualization results of ROI classification. The template user instruction is shown in the blue box. Specifically, given a bounding box prompt, UniBiomed can effectively predict the class of biomedical targets within ROIs. **e.** Comparisons on region-aware report generation in the MedTrinity [15] dataset. We compare UniBiomed with multiple representative MLLMs, including InternVL2.5 [26, 33], LLaVA-Med [12], MedRegA [13], and MedPLIB [14]. We report the results of BLEU [50], METEOR [51], and ROUGE_L [52]. **f.** Radar chart comparisons across different metrics in region-aware report generation. **g.** An example of region-aware report generation on chest x-ray image. The template user instruction is shown in the blue box. The text in green indicates the correct contents. Reference denotes the ground truth from the MedTrinity dataset [15].

The results are shown in **Figure 4 (e) and (f)**. It can be seen that UniBiomed achieves superior performance compared with previous MLLMs [12–14, 26]. Specifically, UniBiomed achieves 52.4%, 30.4%, and 47.9% in BLEU_1, METEOR, and ROUGE_L, respectively, surpassing the best-competing method MedPLIB [14] by 8.8%, 2.3%, and 15.8%. These results robustly validate the effectiveness of UniBiomed in this task. We further present an example of region-aware report generation on prostate pathology images, as shown in **Figure 4 (g)**. It can be seen that UniBiomed can generate a detailed description to illustrate the observed features. More examples are presented in **Extended Data Figure A4**. It can be seen that UniBiomed not only accurately identifies the abnormality (*i.e.*, pneumothorax) within the target regions, but also generates a detailed description to illustrate the observed features. More examples are presented in **Extended Data Figure A4**.

2.6 UniBiomed optimizes biomedical image analysis workflow

In this section, we show that UniBiomed is an effective AI tool for improving the efficiency of the biomedical image analysis workflow. As shown in the upper part of **Figure 5**, previous biomedical segmentation foundation models such as MedSAM [16] and BiomedParse [4] follow a cumbersome process. Given an input CT scan, these models require radiologists to first pre-diagnose each slice to locate target abnormalities, such as liver disease in the example. Once identified, additional manual inputs are necessary, *e.g.*, BiomedParse [4] demands a text description as the textual prompt, while MedSAM [16] relies on a tightly drawn bounding box prompt. More critically,

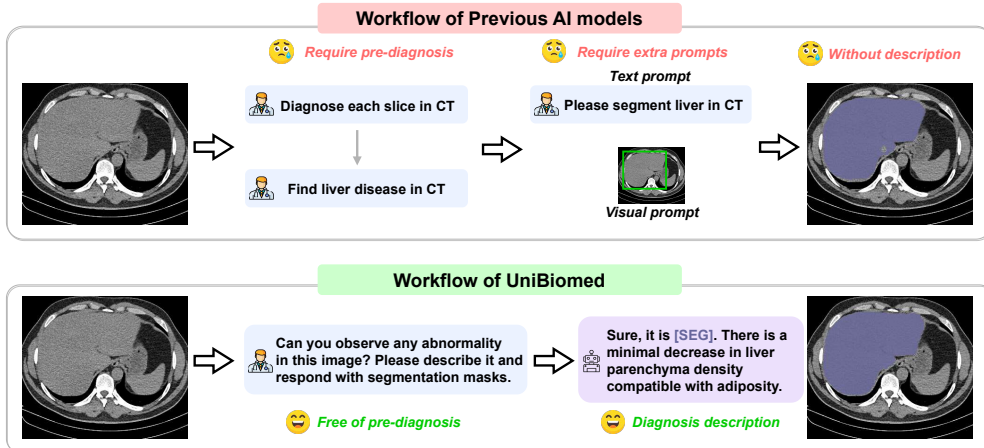


Fig. 5: Workflow comparisons. The upper part presents the workflow of previous biomedical segmentation foundation models, *e.g.*, MedSAM [16] and BiomedParse [4]. The lower part shows the workflow of our introduced UniBiomed. We present an example of grounded report generation on CT images.

these models are limited to segmentation tasks and fail to generate detailed diagnostic descriptions of the targets. These inefficiencies significantly hinder their clinical applications.

In contrast, UniBiomed overcomes these limitations through a novel integration of MLLM and SAM. Given an input CT scan, UniBiomed automatically detects abnormalities, generates precise segmentation masks, and provides detailed diagnostic descriptions. There are two significant advantages in this workflow: (1) First, this process is free of pre-diagnosis by radiologists and requires no manual prompts, eliminating the time-consuming process of slice-by-slice analysis and manual prompt engineering. (2) Moreover, unlike prior foundation models [4, 16, 23, 24], which are limited to segmentation outputs, UniBiomed is capable of combining visual analysis with diagnostic text generation. For example, UniBiomed not only segments targets but also delivers clinically relevant interpretations, such as identifying “a *minimal decrease in liver parenchyma density compatible with adiposity*” as shown in the example. These advancements lead to a significant paradigm shift in biomedical image analysis, which optimizes workflow efficiency and enables an end-to-end diagnosis workflow.

3 Discussion

In this work, we introduce UniBiomed, the first universal foundation model for grounded biomedical image interpretation. UniBiomed effectively unifies the generation of diagnostic findings with the segmentation of corresponding biomedical targets, enabling accurate biomedical image analysis across ten diverse imaging modalities. UniBiomed is based on a novel integration of advanced Multi-modal Large Language

Model (MLLM) and Segment Anything Model (SAM) [27, 28], which can effectively leverage multi-modal biomedical information for tackling diverse biomedical tasks. To develop UniBiomed, we curate a large-scale dataset comprising 27 million triplets of images, region annotations, and text descriptions spanning ten biomedical imaging modalities, which is the largest and most comprehensive dataset for biomedical grounded interpretation. To evaluate the effectiveness of UniBiomed, we conduct a large-scale validation on 70 internal and 14 external datasets with comprehensive comparisons of state-of-the-art methods [4, 12–14, 16, 23, 24, 26, 31, 41]. Extensive experiments demonstrate that UniBiomed achieves state-of-the-art performance on a wide range of biomedical tasks, including biomedical image segmentation, disease recognition, region-aware diagnosis, and report generation. We further showcase that UniBiomed represents a novel paradigm shift in biomedical image analysis workflows, which effectively improves the efficiency of AI-assisted biomedical image analysis. These findings demonstrate the promising prospects of UniBiomed in clinical applications.

Recent advances have attracted increasing attention to multimodal information for biomedical image analysis [8, 12, 42, 47–49, 53]. Concretely, visual features extracted from biomedical images provide anatomical and functional information from cell to organ levels [3–7, 54–56], while textual descriptions from clinical experts offer fine-grained information for interpreting biomedical images [8–10]. Although recent biomedical AI models have showcased encouraging results in biomedical image analysis, it remains challenging to effectively integrate holistic vision and language information for assisting clinicians in practice. Specifically, the clinical adoption of biomedical AI models requires that the AI-generated results are both accurate and interpretable for clinicians to ensure reliability. Thus, it demands that biomedical AI models can output the diagnostic findings and simultaneously highlight the corresponding regions in the images, offering rich visual and textual information for assisting clinicians.

To this end, we underscore the importance of grounded interpretation in biomedical image analysis, *i.e.*, generating diagnostic findings and simultaneously segmenting the corresponding biomedical objects. This task enables models to extract important biomedical targets (*e.g.*, lesions, tumors, cancer cells, or abnormal organs) and generate detailed descriptions (*e.g.*, clinical reports) of corresponding objects to assist clinical experts in diagnosis, unlocking novel opportunities for end-to-end biomedical image analysis.

However, existing biomedical models [3, 4, 12–14, 16, 23, 24, 31, 41, 42, 47, 48, 57] fail to tackle this challenging yet critical task. In particular, grounded interpretation requires simultaneous execution of segmentation and text generation, whereas current models can only conduct these two tasks independently. Concretely, the biomedical segmentation foundation models [4, 16, 23, 24, 57] can deliver segmentation masks while failing to establish text generation tasks such as VQA and report generation. Although recent medical MLLMs [12–14, 42, 47–49] have demonstrated promising results in generating text descriptions for biomedical images, these models are not capable of segmenting the corresponding biomedical objects (*e.g.*, tiny lesions) simultaneously, making it difficult for clinicians to identify the corresponding regions

described in the reports. To illustrate the drawbacks of these methods more clearly, we present a detailed comparison in **Extended Data Table A1**. Compared with previous methods, UniBiomed is the first foundation model to support multi-modal image interpretation, flexible user prompts, segmentation prediction, text description generation, region-aware diagnosis, pixel-level grounding, and end-to-end training in one universal model. This breakthrough paves a promising path towards more accurate and efficient biomedical image analysis.

The ability to leverage different types of biomedical datasets is pivotal to the success of UniBiomed. Previous biomedical foundation models are typically based on disjoint training on separate datasets, *e.g.*, text generation datasets for language models [8, 12] or segmentation datasets for segmentation models [4, 16, 19]. This limitation impedes their ability to leverage holistic vision and language information for biomedical image analysis. In contrast, within a universal training process, UniBiomed can simultaneously leverage image segmentation datasets, vision question answering datasets, report generation datasets, and region-aware diagnosis datasets for developing a strong biomedical foundation model. This distinguished advantage makes UniBiomed stand out from previous biomedical foundation models, achieving better performance across diverse biomedical tasks. We present ablation studies to evaluate the effectiveness of universal training in **Extended Data Figure A2**.

One of the major bottlenecks is the availability of data. To train UniBiomed, the training datasets necessitate both spatial localization and corresponding text descriptions for the biomedical objects. Inspired by the recent advances of “Visual Instruction Tuning” in MLLMs [25, 30, 31], we construct a uniform VQA format to facilitate universal grounded interpretation of biomedical images. In this way, we curate a large-scale dataset comprising 27 million image-text-annotation triplets across ten biomedical imaging modalities for training and validation, which is the largest and most comprehensive dataset in this field. Our curated dataset will fortify the foundation of future research in biomedical grounded interpretation.

We further showcase that UniBiomed is a more practical biomedical AI tool for optimizing workflow efficiency. Prior segmentation foundation models [4, 16, 23, 24] heavily rely on clinical experts to provide accurate textual or visual prompts. Take the representative models, MedSAM [16] and BiomedParse [4] as examples. Both of these models require the users to identify the targets of the input images in advance. Then, visual or textual prompts should be provided, *e.g.*, MedSAM [16] requires tightly drawn bounding boxes as visual prompts while BiomedParse [4] necessitates text instructions from pre-diagnostic findings as textual prompts. This process is tedious for clinicians and significantly hampers workflow efficiency. For example, for 3D medical images like CT and MRI, there are probably a few hundred slices within a scan, while these models [4, 16, 23, 24] require users to pre-diagnose the scans slice-by-slice and provide accurate prompts. In addition, these models [4, 16, 23, 24] still fail to generate diagnostic findings for interpreting the images, which significantly hinders their clinical applications. In contrast, UniBiomed provides automated end-to-end grounded interpretation of biomedical images, with both precise segmentation predictions and detailed text descriptions, which significantly optimizes the workflow efficiency of biomedical image analysis.

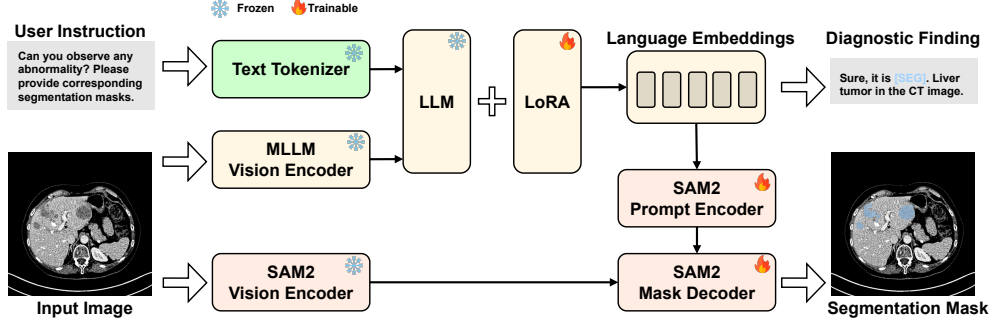


Fig. 6: We present the grounded disease recognition of liver tumors as an example to illustrate the details of UniBiomed. Specifically, the user instruction is processed by a pre-trained text tokenizer BERT [58] and input to LLM. The input image is encoded by the vision encoder of MLLM, then the vision tokens are also injected into LLM for generating the diagnostic findings. Following previous methods [30, 31, 41], we combine the output of the last layer in the MLLM with the tokenized user instructions as the language embeddings and inject them into SAM2’s prompt encoder for producing segmentation masks. Notably, we use LoRA [59] to finetune the MLLM as previous methods [30, 31]. In SAM2, the prompt encoder and mask decoder are fine-tuned, while the vision encoder is frozen.

Although promising results have been demonstrated by UniBiomed, there are still several limitations for further improvement. Despite the extensive scale of our curated dataset, it may still lack incorporation of certain rare diseases or conditions, potentially limiting the model’s generalizability across all medical scenarios. This highlights the need for continuous dataset expansion and diversification to ensure comprehensive biomedical image analysis. In addition, while UniBiomed has achieved satisfactory performance on large-scale public datasets, further exploration of its clinical application is necessary to substantiate the effectiveness of our method. Moving forward, we will work closely with clinical practitioners to ensure that the model addresses practical needs and integrates seamlessly into existing workflows.

4 Methods

4.1 Details of UniBiomed

UniBiomed is based on a novel integration of Multi-modal Large Language Model (MLLM) [25, 26] and the Segment Anything Model (SAM) [27, 28]. Concretely, MLLM is responsible for interpreting multi-modal images and generating text descriptions, while SAM is employed to segment the target biomedical objects based on the given text instructions.

MLLM consists of a vision encoder [60] and a Large Language Model (LLM) [36]. The vision encoder is a typical Vision Transformer (ViT) [60] model, which is pre-trained by CLIP [32] for vision-language alignment [25, 33, 34]. The LLM [36] is responsible for parsing the text instructions from users and generating corresponding

answers. Given an image and a text instruction, the vision encoder encodes the image into visual tokens, while a text tokenizer [58] will process the text into language tokens. These visual and language tokens are then fed into the LLM to generate textual outputs, enabling UniBiomed to tackle diverse text generation tasks.

SAM [27, 28] is further leveraged for tackling the segmentation task, which comprises a vision encoder, a prompt encoder, and a mask decoder. The vision encoder is based on Hiera [61], a hierarchical ViT [60] architecture. The image features extracted by SAM’s vision encoder are passed to the mask decoder, where the prompt encoder encodes the user prompts and prompts the mask encoder to generate segmentation masks. Unlike conventional SAM [27, 28], which relies on visual prompts (*e.g.*, points or bounding boxes), the SAM in UniBiomed is based on the textual prompts generated by MLLM. Following previous methods [30, 31, 41], UniBiomed combines the output of the last layer in the MLLM with the tokenized user instructions as the language embeddings and injects them into SAM’s prompt encoder, enabling text-guided segmentation. This effectively bridges the MLLM and SAM for grounded interpretation [30, 31]. Notably, following the previous methods [30, 31], we adopt a special token “[SEG]” to instruct the mask decoder to produce segmentation masks. While for the tasks that do not require segmentation predictions, *e.g.*, ROI classification and region-aware report generation, this special token is discarded, and the model will not produce segmentation predictions.

Notably, the success of UniBiomed stems from the complementary integration of MLLM and SAM. **First**, unlike the original SAM [27, 28], which relies on visual prompts, UniBiomed employs language embeddings as textual prompts to guide SAM’s mask decoder. This innovation eliminates the need for manually crafting precise bounding boxes—a major bottleneck in segmenting biomedical images with dense, irregularly shaped objects [4]. **Second**, segmentation training in UniBiomed implicitly enhances the diagnostic accuracy of the MLLM [30, 31, 41]. Since segmentation predictions depend on the MLLM’s textual prompts, the back-propagation process propagates supervision signals from the segmentation masks back to the MLLM, refining its ability to generate precise prompts. This synergistic integration not only improves segmentation performance but also strengthens the MLLM’s diagnostic capabilities, creating a mutually reinforcing loop between the two components.

Following the state-of-the-art architecture Sa2VA [30], we adopt InternVL2.5 [26] as the foundation MLLM and SAM2-hiera-large [28] as the segmentation model. To preserve the learned knowledge of the strong pre-trained MLLM, we leverage LoRA [59] to perform efficient fine-tuning of LLM, and freeze the vision encoder of MLLM entirely. For SAM2 [28], following previous settings [30, 31], we freeze the vision encoder and fine-tune the prompt encoder and mask decoder only.

We aggregate different sources of datasets into a universal training process. The overall training loss consists of a text generation loss L_{text} and a segmentation loss L_{seg} . The text generation loss L_{text} is an auto-regressive cross-entropy loss as standard LLM [25, 30, 31]. The segmentation loss L_{seg} is a combination of per-pixel binary cross-entropy (BCE) loss L_{BCE} and typical dice loss L_{dice} . We balance the weights of

loss functions, and the overall loss L is defined as:

$$L = L_{text} + L_{seg}, \quad L_{seg} = \lambda_{BCE} * L_{BCE} + \lambda_{dice} * L_{dice}. \quad (1)$$

Following previous methods [4, 30, 31], the coefficient of loss functions λ_{BCE} and λ_{dice} are defined as 2 and 0.5, respectively. The per-pixel binary cross-entropy (BCE) loss L_{BCE} is defined as:

$$L_{BCE} = -\frac{1}{N} \sum_{i=1}^N [y_i \log(p_i) + (1 - y_i) \log(1 - p_i)] \quad (2)$$

where $y_i \in \{0, 1\}$ is the ground truth label, $p_i \in [0, 1]$ is the predicted probability, and N is the total number of pixels. The dice loss L_{dice} is given by:

$$L_{dice} = 1 - \frac{2 \sum_{i=1}^N p_i y_i + \epsilon}{\sum_{i=1}^N p_i + \sum_{i=1}^N y_i + \epsilon} \quad (3)$$

where ϵ is a small constant for numerical stability.

Specifically, for the ROI classification and region-aware report generation tasks, the L_{seg} will be discarded during training. In this case, the loss function L is formulated as:

$$L = L_{text}. \quad (4)$$

4.2 Implementation

For dataset curation, we adopt some readily available toolkits from SA2VA [30], RadGenome [43], VoCo [62, 63], BiomedParse [4], and MedTrinity [15] to transform the datasets into a uniform VQA format. Some examples are shown in **Extended Data Figure A3**. For fair comparisons, we resize all images to 1024×1024 sizes for training and validation. We use Pytorch [64] to conduct all training and validation experiments. The training of UniBiomed is conducted on $8 \times$ NVIDIA H800 (80G) GPUs for 10 epochs, which takes about 5 days to finish the training. All the inference tasks can be established within one NVIDIA 3090 GPU (24GB). We provide the available code links of comparison methods in **Extended Data Table A7**. More details of training and validation are shown in **Extended Data Table A8**.

4.3 Evaluation

Following previous methods [4, 16], we did not conduct validation during training to select hyperparameters for fair comparisons. For evaluation, we strictly split the internal datasets into 80% training and 20% test sets as previous method [4] for fair comparisons. To avoid information leakage, all the external datasets are unseen in the training of our method and all comparison methods, and we conduct direct inference on these datasets.

Comparison methods. In this work, we focus on evaluating the effectiveness of grounded interpretation. Thus, we compare segmentation foundation models on segmentation tasks and compare medical MLLMs on medical diagnosis tasks.

We first compare MedSAM [16], BiomedParse [4], SegVol [23], and SAT [24] in the biomedical image segmentation task. Specifically, MedSAM, BiomedParse, SegVol, and SAT are generalist models that can be applied to multiple datasets. MedSAM and SegVol adopt visual prompts while BiomedParse and SAT use textual prompts for segmentation. SegVol and SAT are only applicable to 3D medical images like CT and MRI, which are not available for multi-modal biomedical images. In addition, the methods based on visual prompts, MedSAM and SegVol, are not applicable to the biomedical objects with irregular shapes [4]. Most of the segmentation datasets used in our method have already been trained in these models. **For fair comparisons, we fine-tune these models on the internal segmentation datasets used in our method.** We conduct five experimental runs and report the confidence ranges to ensure reliable results. The details of datasets are shown in **Extended Data Table A2**.

For the text generation task, we first compare GLaMM [41] and LISA [31] in grounded disease recognition and grounded report generation. Specifically, we re-implement these methods on our curated datasets for fair comparisons. The details of datasets for grounded disease recognition are shown in **Extended Data Table A6**. We evaluate the performance of grounded report generation on the RadGenome [29, 43] dataset.

Then, we compare MedRegA [13] and MedPLIB [14] in ROI classification. These two medical MLLMs [13, 14] have been trained on large-scale ROI classification datasets. For fair comparisons, we further fine-tune them on our dataset to ensure the training datasets are consistent. Following MedPLIB [14], for ROI classification, we degrade the segmentation masks of segmentation datasets to bounding boxes as visual prompts for representing the ROIs, then predict the biomedical classes within the ROIs. Following ViP-LLaVA [45], we directly overlay bounding boxes onto the biomedical images, eliminating the need for complex region encodings for indicating ROIs. The datasets for ROI classification are shown in **Extended Data Table A2**.

Furthermore, we compare InternVL2.5 [26], LLaVA-Med [12], MedRegA [13], and MedPLIB [14] in region-aware report generation. Notably, the medical MLLMs [12–14] are trained on the VQA and report generation datasets used in this method, enabling us to conduct fair comparisons. We report the results on the MedTrinity [15] dataset. Specifically, the MedTrinity dataset is aggregated from 23 report generation datasets, as shown in **Extended Data Table A3**. In this work, we report the overall results on the whole MedTrinity dataset instead of the separate datasets.

Evaluation metrics. For the evaluation of segmentation, the standard Dice score (%) is employed to evaluate the performance. Dice score is calculated as:

$$\text{Dice}(P, G) = \frac{2|P \cap G|}{|P| + |G|}, \quad (5)$$

where P denotes the segmentation predictions, G is the ground truth of segmentation labels.

For the task of grounded disease recognition, we present the results of both dice scores and accuracy. The accuracy is calculated as:

$$\text{Accuracy} = \frac{1}{N} \sum_{i=1}^N 1(y_i = \hat{y}_i), \quad (6)$$

where N is the total number of samples. y and \hat{y} are the predictions and labels, respectively. $1(y_i = \hat{y}_i)$ denotes that the prediction of i_{th} sample is correct.

For the task of ROI classification, we simply use the accuracy metric to measure the performance. As for the region-aware report generation task, we further employ Bilingual Evaluation Understudy (BLEU) [50], Metric for Evaluation of Translation with Explicit ORdering (METEOR) [51], and Recall-Oriented Understudy for Gisting Evaluation with Longest Common Subsequence (ROUGE-L) [52] for evaluation.

Specifically, the formulation of BLEU is as follows:

$$\text{BLEU} = BP \cdot \exp \left(\sum_{n=1}^N w_n \log p_n \right), \quad (7)$$

where BP is the brevity penalty, p_n are modified n-gram precisions, and w_n are weights. The BLEU variants, *i.e.*, BLEU1, BLEU2, BLEU3, and BLEU4 are differ in their n-gram scope:

$$\text{BLEU-1} = BP \cdot \exp(\log p_1), \quad (8)$$

$$\text{BLEU-2} = BP \cdot \exp \left(\frac{1}{2} \sum_{n=1}^2 \log p_n \right), \quad (9)$$

$$\text{BLEU-3} = BP \cdot \exp \left(\frac{1}{3} \sum_{n=1}^3 \log p_n \right), \quad (10)$$

$$\text{BLEU-4} = BP \cdot \exp \left(\frac{1}{4} \sum_{n=1}^4 \log p_n \right). \quad (11)$$

The METEOR [51] is an automatic evaluation metric for evaluating the quality of machine translation, which not only considers vocabulary matching but also combines word order similarity and alignment information. It is calculated as:

$$\text{METEOR} = \frac{1}{m} \cdot \sum_{g \in \text{gold}} \max_{h \in \text{hyp}} \text{Precision}(g, h), \quad (12)$$

where m is the number of gold standard (reference) sentences, and $\text{Precision}(g, h)$ refers to the precision score between a specific gold standard sentence (g) and a hypothesis sentence (h) from the set of all gold standard sentences (gold) and the set of all hypothesis sentences (hyp).

ROUGE-L is an automatic evaluation metric for assessing machine-generated text by measuring the longest common subsequence (LCS) between the hypothesis and reference. It computes recall, precision, and their harmonic mean (F-score) as follows:

$$R_{\text{LCS}} = \frac{\text{LCS}(X, Y)}{|Y|}, \quad P_{\text{LCS}} = \frac{\text{LCS}(X, Y)}{|X|}, \quad F_{\text{LCS}} = \frac{(1 + \beta^2)R_{\text{LCS}}P_{\text{LCS}}}{R_{\text{LCS}} + \beta^2P_{\text{LCS}}}, \quad (13)$$

where X is the hypothesis, Y is the reference, and β controls recall emphasis. For multiple references, it averages the best F_{LCS} across pairs, similar to METEOR in Equation 12. Unlike METEOR, it ignores synonyms and alignment, focusing on word-order-agnostic overlap.

For the grounded report generation evaluation, we also use (BLEU) [50], METEOR [51], and ROUGE-L [52] as the metrics. In addition, we further use dice scores to measure the performance of segmentation.

5 Data availability

This study incorporates a total of 84 datasets across 10 diverse biomedical imaging modalities. All these datasets are publicly available for research. For detailed information about the data used in this project, please refer to **Extended Data Tables A2, A3, A4, and A5**.

6 Code availability

The codes, datasets, and models of UniBiomed is available at GitHub (<https://github.com/Luffy03/UniBiomed>).

7 Author contributions

L.W. designed the framework and conducted the experiments. Y.N., S.H., and J.Z. contributed to the data acquisition and provided suggestions on the framework. N.M., V.V., and R.C.K.C. contributed to the clinician evaluation and analyzed the results of UniBiomed. Y.P. and P.R. polished the manuscript and provided suggestions on the experiments. H.C. conceived and supervised the work. All authors discussed the results and contributed to the final manuscript.

Declaration

The authors have no conflicts of interest to declare.

Ethics declaration

This project has been reviewed and approved by the Human and Artefacts Research Ethics Committee (HAREC). The protocol number is HREP-2025-0188.

Acknowledgements

This work was supported by the Hong Kong Innovation and Technology Commission (Project No. MHP/002/22, GHP/006/22GD and ITCPD/17-9), HKUST (Project No. FS111), and the Research Grants Council of the Hong Kong Special Administrative Region, China (Project Reference Number: T45-401/22-N). We also thank the support of HKUST SuperPOD for providing the GPU platform for model training.

References

- [1] Royer, L.A.: The future of bioimage analysis: a dialog between mind and machine. *Nature Methods* **20**(7), 951–952 (2023)
- [2] Li, X., Zhang, Y., Wu, J., Dai, Q.: Challenges and opportunities in bioimage analysis. *Nature Methods* **20**(7), 958–961 (2023)
- [3] Isensee, F., Jaeger, P.F., Kohl, S.A., Petersen, J., Maier-Hein, K.H.: nnu-net: a self-configuring method for deep learning-based biomedical image segmentation. *Nature Methods* **18**(2), 203–211 (2021)
- [4] Zhao, T., Gu, Y., Yang, J., Usuyama, N., Lee, H.H., Kiblawi, S., Naumann, T., Gao, J., Crabtree, A., Abel, J., Moungh-Wen, C., Piening, B., Bifulco, C., Wei, M., Poon, H., Wang, S.: A foundation model for joint segmentation, detection, and recognition of biomedical objects across nine modalities. *Nature Methods* (2024) <https://doi.org/10.1038/s41592-024-02499-w>
- [5] Xu, H., Usuyama, N., Bagga, J., Zhang, S., Rao, R., Naumann, T., Wong, C., Gero, Z., González, J., Gu, Y., *et al.*: A whole-slide foundation model for digital pathology from real-world data. *Nature* **630**(8015), 181–188 (2024)
- [6] Sun, Y., Wang, L., Li, G., Lin, W., Wang, L.: A foundation model for enhancing magnetic resonance images and downstream segmentation, registration and diagnostic tasks. *Nature Biomedical Engineering*, 1–18 (2024)
- [7] Antonelli, M., Reinke, A., Bakas, S., Farahani, K., Kopp-Schneider, A., Landman, B.A., Litjens, G., Menze, B., Ronneberger, O., Summers, R.M., *et al.*: The medical segmentation decathlon. *Nature Communications* **13**(1), 4128 (2022)
- [8] Zhang, K., Zhou, R., Adhikarla, E., Yan, Z., Liu, Y., Yu, J., Liu, Z., Chen, X., Davison, B.D., Ren, H., *et al.*: A generalist vision–language foundation model for diverse biomedical tasks. *Nature Medicine*, 1–13 (2024)
- [9] Peng, Y., Rousseau, J.F., Shortliffe, E.H., Weng, C.: Ai-generated text may have a role in evidence-based medicine. *Nature Medicine* **29**(7), 1593–1594 (2023)
- [10] Lu, M.Y., Chen, B., Williamson, D.F., Chen, R.J., Zhao, M., Chow, A.K., Ike-mura, K., Kim, A., Pouli, D., Patel, A., *et al.*: A multimodal generative ai copilot

- for human pathology. *Nature*, 1–3 (2024)
- [11] Kim, C., Gadgil, S.U., DeGrave, A.J., Omiye, J.A., Cai, Z.R., Daneshjou, R., Lee, S.-I.: Transparent medical image ai via an image-text foundation model grounded in medical literature. *Nature Medicine* **30**(4), 1154–1165 (2024)
 - [12] Li, C., Wong, C., Zhang, S., Usuyama, N., Liu, H., Yang, J., Naumann, T., Poon, H., Gao, J.: Llava-med: Training a large language-and-vision assistant for biomedicine in one day. *Advances in Neural Information Processing Systems* **36**, 28541–28564 (2023)
 - [13] Wang, L., Wang, H., Yang, H., Mao, J., Yang, Z., Shen, J., Li, X.: Interpretable bilingual multimodal large language model for diverse biomedical tasks. In: *International Conference on Learning Representations* (2025)
 - [14] Huang, X., Shen, L., Liu, J., Shang, F., Li, H., Huang, H., Yang, Y.: Towards a multimodal large language model with pixel-level insight for biomedicine. In: *Proceedings of the AAAI Conference on Artificial Intelligence*, vol. 39, pp. 3779–3787 (2025)
 - [15] Xie, Y., Zhou, C., Gao, L., Wu, J., Li, X., Zhou, H.-Y., Liu, S., Xing, L., Zou, J., Xie, C., *et al.*: Medtrinity-25m: A large-scale multimodal dataset with multi-granular annotations for medicine. In: *International Conference on Learning Representations* (2025)
 - [16] Ma, J., He, Y., Li, F., Han, L., You, C., Wang, B.: Segment anything in medical images. *Nature Communications* **15**(1), 654 (2024)
 - [17] Wang, G., Liu, X., Shen, J., Wang, C., Li, Z., Ye, L., Wu, X., Chen, T., Wang, K., Zhang, X., *et al.*: A deep-learning pipeline for the diagnosis and discrimination of viral, non-viral and covid-19 pneumonia from chest x-ray images. *Nature Biomedical Engineering* **5**(6), 509–521 (2021)
 - [18] Archit, A., Freckmann, L., Nair, S., Khalid, N., Hilt, P., Rajashekar, V., Freitag, M., Teuber, C., Buckley, G., Haaren, S., *et al.*: Segment anything for microscopy. *Nature Methods*, 1–13 (2025)
 - [19] Stringer, C., Wang, T., Michaelos, M., Pachitariu, M.: Cellpose: a generalist algorithm for cellular segmentation. *Nature methods* **18**(1), 100–106 (2021)
 - [20] Pachitariu, M., Stringer, C.: Cellpose 2.0: how to train your own model. *Nature methods* **19**(12), 1634–1641 (2022)
 - [21] Stringer, C., Pachitariu, M.: Cellpose3: one-click image restoration for improved cellular segmentation. *Nature Methods*, 1–8 (2025)
 - [22] Peiris, H., Hayat, M., Chen, Z., Egan, G., Harandi, M.: Uncertainty-guided

- dual-views for semi-supervised volumetric medical image segmentation. *Nature Machine Intelligence* **5**(7), 724–738 (2023)
- [23] Du, Y., Bai, F., Huang, T., Zhao, B.: Segvol: Universal and interactive volumetric medical image segmentation. *Advances in Neural Information Processing Systems* **37**, 110746–110783 (2024)
 - [24] Zhao, Z., Zhang, Y., Wu, C., Zhang, X., Zhang, Y., Wang, Y., Xie, W.: One model to rule them all: Towards universal segmentation for medical images with text prompts. *arXiv preprint arXiv:2312.17183* (2023)
 - [25] Liu, H., Li, C., Wu, Q., Lee, Y.J.: Visual instruction tuning. *Advances in Neural Information Processing Systems* **36**, 34892–34916 (2023)
 - [26] Chen, Z., Wang, W., Cao, Y., Liu, Y., Gao, Z., Cui, E., Zhu, J., Ye, S., Tian, H., Liu, Z., et al.: Expanding performance boundaries of open-source multimodal models with model, data, and test-time scaling. *arXiv preprint arXiv:2412.05271* (2024)
 - [27] Kirillov, A., Mintun, E., Ravi, N., Mao, H., Rolland, C., Gustafson, L., Xiao, T., Whitehead, S., Berg, A.C., Lo, W.-Y., et al.: Segment anything. In: *Proceedings of the IEEE/CVF International Conference on Computer Vision*, pp. 4015–4026 (2023)
 - [28] Ravi, N., Gabeur, V., Hu, Y.-T., Hu, R., Ryali, C., Ma, T., Khedr, H., Rädle, R., Rolland, C., Gustafson, L., et al.: Sam 2: Segment anything in images and videos. *International Conference on Learning Representations* (2024)
 - [29] Hamamci, I.E., Er, S., Almas, F., Simsek, A.G., Esirgun, S.N., Dogan, I., Dasdelen, M.F., Wittmann, B., Simsar, E., Simsar, M., et al.: A foundation model utilizing chest ct volumes and radiology reports for supervised-level zero-shot detection of abnormalities. *arXiv preprint arXiv:2403.17834* (2024)
 - [30] Yuan, H., Li, X., Zhang, T., Huang, Z., Xu, S., Ji, S., Tong, Y., Qi, L., Feng, J., Yang, M.-H.: Sa2va: Marrying sam2 with llava for dense grounded understanding of images and videos. *arXiv preprint arXiv:2501.04001* (2025)
 - [31] Lai, X., Tian, Z., Chen, Y., Li, Y., Yuan, Y., Liu, S., Jia, J.: Lisa: Reasoning segmentation via large language model. In: *Proceedings of the IEEE/CVF Conference on Computer Vision and Pattern Recognition*, pp. 9579–9589 (2024)
 - [32] Radford, A., Kim, J.W., Hallacy, C., Ramesh, A., Goh, G., Agarwal, S., Sastry, G., Askell, A., Mishkin, P., Clark, J., et al.: Learning transferable visual models from natural language supervision. In: *International Conference on Machine Learning*, pp. 8748–8763 (2021). PmLR
 - [33] Chen, Z., Wu, J., Wang, W., Su, W., Chen, G., Xing, S., Zhong, M., Zhang, Q.,

- Zhu, X., Lu, L., *et al.*: Internvl: Scaling up vision foundation models and aligning for generic visual-linguistic tasks. In: Proceedings of the IEEE/CVF Conference on Computer Vision and Pattern Recognition, pp. 24185–24198 (2024)
- [34] Bai, J., Bai, S., Yang, S., Wang, S., Tan, S., Wang, P., Lin, J., Zhou, C., Zhou, J.: Qwen-vl: A versatile vision-language model for understanding, localization, text reading, and beyond. arXiv preprint arXiv:2308.12966 (2023)
- [35] Li, J., Li, D., Savarese, S., Hoi, S.: Blip-2: Bootstrapping language-image pre-training with frozen image encoders and large language models. In: International Conference on Machine Learning, pp. 19730–19742 (2023). PMLR
- [36] Touvron, H., Lavril, T., Izacard, G., Martinet, X., Lachaux, M.-A., Lacroix, T., Rozière, B., Goyal, N., Hambro, E., Azhar, F., *et al.*: Llama: Open and efficient foundation language models. arXiv preprint arXiv:2302.13971 (2023)
- [37] Liu, S., Zeng, Z., Ren, T., Li, F., Zhang, H., Yang, J., Jiang, Q., Li, C., Yang, J., Su, H., *et al.*: Grounding dino: Marrying dino with grounded pre-training for open-set object detection. In: European Conference on Computer Vision, pp. 38–55 (2024). Springer
- [38] Li, L.H., Zhang, P., Zhang, H., Yang, J., Li, C., Zhong, Y., Wang, L., Yuan, L., Zhang, L., Hwang, J.-N., *et al.*: Grounded language-image pre-training. In: Proceedings of the IEEE/CVF Conference on Computer Vision and Pattern Recognition, pp. 10965–10975 (2022)
- [39] Zou, X., Yang, J., Zhang, H., Li, F., Li, L., Wang, J., Wang, L., Gao, J., Lee, Y.J.: Segment everything everywhere all at once. *Advances in Neural Information Processing Systems* **36**, 19769–19782 (2023)
- [40] Zhang, T., Li, X., Fei, H., Yuan, H., Wu, S., Ji, S., Loy, C.C., Yan, S.: Omg-llava: Bridging image-level, object-level, pixel-level reasoning and understanding. *Advances in Neural Information Processing Systems* **37**, 71737–71767 (2024)
- [41] Rasheed, H., Maaz, M., Shaji, S., Shaker, A., Khan, S., Cholakkal, H., Anwer, R.M., Xing, E., Yang, M.-H., Khan, F.S.: Glamm: Pixel grounding large multi-modal model. In: Proceedings of the IEEE/CVF Conference on Computer Vision and Pattern Recognition, pp. 13009–13018 (2024)
- [42] Bai, F., Du, Y., Huang, T., Meng, M.Q.-H., Zhao, B.: M3d: Advancing 3d medical image analysis with multi-modal large language models. arXiv preprint arXiv:2404.00578 (2024)
- [43] Zhang, X., Wu, C., Zhao, Z., Lei, J., Zhang, Y., Wang, Y., Xie, W.: Radgenome-chest ct: A grounded vision-language dataset for chest ct analysis. arXiv preprint arXiv:2404.16754 (2024)

- [44] Yuan, Y., Li, W., Liu, J., Tang, D., Luo, X., Qin, C., Zhang, L., Zhu, J.: Osprey: Pixel understanding with visual instruction tuning. In: Proceedings of the IEEE/CVF Conference on Computer Vision and Pattern Recognition, pp. 28202–28211 (2024)
- [45] Cai, M., Liu, H., Mustikovela, S.K., Meyer, G.P., Chai, Y., Park, D., Lee, Y.J.: Vip-llava: Making large multimodal models understand arbitrary visual prompts. In: Proceedings of the IEEE/CVF Conference on Computer Vision and Pattern Recognition, pp. 12914–12923 (2024)
- [46] Tanida, T., Müller, P., Kaissis, G., Rueckert, D.: Interactive and explainable region-guided radiology report generation. In: Proceedings of the IEEE/CVF Conference on Computer Vision and Pattern Recognition, pp. 7433–7442 (2023)
- [47] Wu, C., Zhang, X., Zhang, Y., Wang, Y., Xie, W.: Towards generalist foundation model for radiology by leveraging web-scale 2d&3d medical data. arXiv preprint arXiv:2308.02463 (2023)
- [48] Shui, Z., Zhang, J., Cao, W., Wang, S., Guo, R., Lu, L., Yang, L., Ye, X., Liang, T., Zhang, Q., *et al.*: Large-scale and fine-grained vision-language pre-training for enhanced ct image understanding. In: International Conference on Learning Representations (2025)
- [49] He, S., Nie, Y., Wang, H., Yang, S., Wang, Y., Cai, Z., Chen, Z., Xu, Y., Luo, L., Xiang, H., *et al.*: Gsco: Towards generalizable ai in medicine via generalist-specialist collaboration. arXiv preprint arXiv:2404.15127 (2024)
- [50] Papineni, K., Roukos, S., Ward, T., Zhu, W.-J.: Bleu: a method for automatic evaluation of machine translation. In: Proceedings of the 40th Annual Meeting of the Association for Computational Linguistics, pp. 311–318 (2002)
- [51] Banerjee, S., Lavie, A.: Meteor: An automatic metric for mt evaluation with improved correlation with human judgments. In: Proceedings of the Acl Workshop on Intrinsic and Extrinsic Evaluation Measures for Machine Translation And/or Summarization, pp. 65–72 (2005)
- [52] Lin, C.-Y.: Rouge: A package for automatic evaluation of summaries. In: Text Summarization Branches Out, pp. 74–81 (2004)
- [53] Nie, Y., He, S., Bie, Y., Wang, Y., Chen, Z., Yang, S., Chen, H.: Conceptclip: Towards trustworthy medical ai via concept-enhanced contrastive language-image pre-training. arXiv preprint arXiv:2501.15579 (2025)
- [54] Wu, L., Zhuang, J., Ni, X., Chen, H.: Freetumor: Advance tumor segmentation via large-scale tumor synthesis. arXiv preprint arXiv:2406.01264 (2024)
- [55] Zhuang, J., Wu, L., Wang, Q., Vardhanabhuti, V., Luo, L., Chen, H.: Mim:

- Mask in mask self-supervised pre-training for 3d medical image analysis. arXiv preprint arXiv:2404.15580 (2024)
- [56] Wu, L., Zhuang, J., Zhou, Y., He, S., Ma, J., Luo, L., Wang, X., Ni, X., Zhong, X., Wu, M., et al.: Freetumor: Large-scale generative tumor synthesis in computed tomography images for improving tumor recognition. arXiv preprint arXiv:2502.18519 (2025)
 - [57] Zhu, J., Qi, Y., Wu, J.: Medical sam 2: Segment medical images as video via segment anything model 2. arXiv preprint arXiv:2408.00874 (2024)
 - [58] Devlin, J., Chang, M.-W., Lee, K., Toutanova, K.: Bert: Pre-training of deep bidirectional transformers for language understanding. In: Proceedings of the 2019 Conference of the North American Chapter of the Association for Computational Linguistics: Human Language Technologies, Volume 1 (long and Short Papers), pp. 4171–4186 (2019)
 - [59] Hu, E.J., Shen, Y., Wallis, P., Allen-Zhu, Z., Li, Y., Wang, S., Wang, L., Chen, W., et al.: Lora: Low-rank adaptation of large language models. International Conference on Learning Representations **1**(2), 3 (2022)
 - [60] Dosovitskiy, A., Beyer, L., Kolesnikov, A., Weissenborn, D., Zhai, X., Unterthiner, T., Dehghani, M., Minderer, M., Heigold, G., Gelly, S., et al.: An image is worth 16x16 words: Transformers for image recognition at scale. In: International Conference on Learning Representations (2020)
 - [61] Ryali, C., Hu, Y.-T., Bolya, D., Wei, C., Fan, H., Huang, P.-Y., Aggarwal, V., Chowdhury, A., Poursaeed, O., Hoffman, J., et al.: Hiera: A hierarchical vision transformer without the bells-and-whistles. In: International Conference on Machine Learning, pp. 29441–29454 (2023). PMLR
 - [62] Wu, L., Zhuang, J., Chen, H.: Large-scale 3d medical image pre-training with geometric context priors. arXiv preprint arXiv:2410.09890 (2024)
 - [63] Wu, L., Zhuang, J., Chen, H.: Voco: A simple-yet-effective volume contrastive learning framework for 3d medical image analysis. In: Proceedings of the IEEE/CVF Conference on Computer Vision and Pattern Recognition, pp. 22873–22882 (2024)
 - [64] Paszke, A., Gross, S., Massa, F., Lerer, A., Bradbury, J., Chanan, G., Killeen, T., Lin, Z., Gimelshein, N., Antiga, L., et al.: Pytorch: An imperative style, high-performance deep learning library. Advances in Neural Information Processing Systems **32** (2019)
 - [65] Gong, S., Zhong, Y., Ma, W., Li, J., Wang, Z., Zhang, J., Heng, P.-A., Dou, Q.: 3dsam-adapter: Holistic adaptation of sam from 2d to 3d for promptable tumor segmentation. Medical Image Analysis **98**, 103324 (2024)

- [66] Jaeger, S., Candemir, S., Antani, S., Wáng, Y.-X.J., Lu, P.-X., Thoma, G.: Two public chest x-ray datasets for computer-aided screening of pulmonary diseases. *Quantitative imaging in medicine and surgery* **4**(6), 475 (2014)
- [67] Chowdhury, M.E., Rahman, T., Khandakar, A., Mazhar, R., Kadir, M.A., Mahbub, Z.B., Islam, K.R., Khan, M.S., Iqbal, A., Al Emadi, N., *et al.*: Can ai help in screening viral and covid-19 pneumonia? *IEEE Access* **8**, 132665–132676 (2020)
- [68] Tahir, A.M., Chowdhury, M.E., Khandakar, A., Rahman, T., Qiblawey, Y., Khurshid, U., Kiranyaz, S., Ibtehaz, N., Rahman, M.S., Al-Maadeed, S., *et al.*: Covid-19 infection localization and severity grading from chest x-ray images. *Computers in biology and medicine* **139**, 105002 (2021)
- [69] Khaled, R., *et al.*: Categorized digital database for low energy and subtracted contrast enhanced spectral mammography images. *The Cancer Imaging Archive* (2021)
- [70] Sae-Lim, W., Wettayaprasit, W., Suwannanon, R., Cheewatanakornkul, S., Aiyarak, P.: Automated pneumothorax segmentation and quantification algorithm based on deep learning. *Intelligent Systems with Applications* **22**, 200383 (2024)
- [71] Gamper, J., Koohbanani, N.A., Benes, K., Graham, S., Jahanifar, M., Khurram, S.A., Azam, A., Hewitt, K., Rajpoot, N.: Pannuke dataset extension, insights and baselines. *arXiv preprint arXiv:2003.10778* (2020)
- [72] Sirinukunwattana, K., Pluim, J.P., Chen, H., Qi, X., Heng, P.-A., Guo, Y.B., Wang, L.Y., Matuszewski, B.J., Bruni, E., Sanchez, U., *et al.*: Gland segmentation in colon histology images: The glas challenge contest. *Medical Image Analysis* **35**, 489–502 (2017)
- [73] Sitnik, D., Aralica, G., Hadžija, M., Hadžija, M.P., Pačić, A., Periša, M.M., Manojlović, L., Krstanac, K., Plavetić, A., Kopriva, I.: A dataset and a methodology for intraoperative computer-aided diagnosis of a metastatic colon cancer in a liver. *Biomedical Signal Processing and Control* **66**, 102402 (2021)
- [74] Mahbod, A., Schaefer, G., Bancher, B., Löw, C., Dorffner, G., Ecker, R., Ellinger, I.: Cryonuseg: A dataset for nuclei instance segmentation of cryosectioned h&e-stained histological images. *Computers in biology and medicine* **132**, 104349 (2021)
- [75] Da, Q., Huang, X., Li, Z., Zuo, Y., Zhang, C., Liu, J., Chen, W., Li, J., Xu, D., Hu, Z., *et al.*: Digestpath: A benchmark dataset with challenge review for the pathological detection and segmentation of digestive-system. *Medical Image Analysis* **80**, 102485 (2022)
- [76] Silva-Rodríguez, J., Colomer, A., Sales, M.A., Molina, R., Naranjo, V.: Going

- deeper through the gleason scoring scale: An automatic end-to-end system for histology prostate grading and cribriform pattern detection. *Computer Methods and Programs in Biomedicine* **195**, 105637 (2020)
- [77] Han, C., Lin, J., Mai, J., Wang, Y., Zhang, Q., Zhao, B., Chen, X., Pan, X., Shi, Z., Xu, Z., *et al.*: Multi-layer pseudo-supervision for histopathology tissue semantic segmentation using patch-level classification labels. *Medical Image Analysis* **80**, 102487 (2022)
 - [78] Graham, S., Chen, H., Gamper, J., Dou, Q., Heng, P.-A., Snead, D., Tsang, Y.W., Rajpoot, N.: Mild-net: Minimal information loss dilated network for gland instance segmentation in colon histology images. *Medical Image Analysis* **52**, 199–211 (2019)
 - [79] Kumar, N., Verma, R., Anand, D., Zhou, Y., Onder, O.F., Tsougenis, E., Chen, H., Heng, P.-A., Li, J., Hu, Z., *et al.*: A multi-organ nucleus segmentation challenge. *IEEE Transactions on Medical Imaging* **39**(5), 1380–1391 (2019)
 - [80] Vitale, S., Orlando, J.I., Iarussi, E., Larrabide, I.: Improving realism in patient-specific abdominal ultrasound simulation using cyclegans. *International Journal of Computer Assisted Radiology and Surgery* **15**(2), 183–192 (2020)
 - [81] Leclerc, S., Smistad, E., Pedrosa, J., Østvik, A., Cervenansky, F., Espinosa, F., Espeland, T., Berg, E.A.R., Jodoin, P.-M., Grenier, T., *et al.*: Deep learning for segmentation using an open large-scale dataset in 2d echocardiography. *IEEE Transactions on Medical Imaging* **38**(9), 2198–2210 (2019)
 - [82] Jieyun, B., ZhanHong, O.: Pubic symphysis-fetal head segmentation and angle of progression (2024)
 - [83] Orlando, J.I., Fu, H., Breda, J.B., Van Keer, K., Bathula, D.R., Diaz-Pinto, A., Fang, R., Heng, P.-A., Kim, J., Lee, J., *et al.*: Refuge challenge: A unified framework for evaluating automated methods for glaucoma assessment from fundus photographs. *Medical Image Analysis* **59**, 101570 (2020)
 - [84] Staal, J., Abràmoff, M.D., Niemeijer, M., Viergever, M.A., Van Ginneken, B.: Ridge-based vessel segmentation in color images of the retina. *IEEE Transactions on Medical Imaging* **23**(4), 501–509 (2004)
 - [85] Amelard, R., Glaister, J., Wong, A., Clausi, D.A.: High-level intuitive features (hlifs) for intuitive skin lesion description. *IEEE Transactions on Biomedical Engineering* **62**(3), 820–831 (2014)
 - [86] Ngoc Lan, P., An, N.S., Hang, D.V., Long, D.V., Trung, T.Q., Thuy, N.T., Sang, D.V.: Neounet: Towards accurate colon polyp segmentation and neoplasm detection. In: *Advances in Visual Computing: 16th International Symposium, ISVC 2021, Virtual Event, October 4-6, 2021, Proceedings, Part II*, pp. 15–28

(2021). Springer

- [87] Ahmed, Z., Panhwar, S.Q., Baqai, A., Umrani, F.A., Ahmed, M., Khan, A.: Deep learning based automated detection of intraretinal cystoid fluid. *International Journal of Imaging Systems and Technology* **32**(3), 902–917 (2022)
- [88] Ji, Y., Bai, H., Ge, C., Yang, J., Zhu, Y., Zhang, R., Li, Z., Zhanng, L., Ma, W., Wan, X., *et al.*: Amos: A large-scale abdominal multi-organ benchmark for versatile medical image segmentation. *Advances in Neural Information Processing Systems* **35**, 36722–36732 (2022)
- [89] Landman, B., Xu, Z., Igelsias, J., Styner, M., Langerak, T., Klein, A.: Miccai multi-atlas labeling beyond the cranial vault—workshop and challenge. In: *Proc. MICCAI Multi-Atlas Labeling Beyond Cranial Vault—Workshop Challenge*, vol. 5, p. 12 (2015)
- [90] Luo, X., Liao, W., Xiao, J., Chen, J., Song, T., Zhang, X., Li, K., Metaxas, D.N., Wang, G., Zhang, S.: Word: A large scale dataset, benchmark and clinical applicable study for abdominal organ segmentation from ct image. *Medical Image Analysis* **82**, 102642 (2022)
- [91] Ma, J., Zhang, Y., Gu, S., An, X., Wang, Z., Ge, C., Wang, C., Zhang, F., Wang, Y., Xu, Y., *et al.*: Fast and low-gpu-memory abdomen ct organ segmentation: the flare challenge. *Medical Image Analysis* **82**, 102616 (2022)
- [92] Heller, N., Isensee, F., Trofimova, D., Tejpaul, R., Zhao, Z., Chen, H., Wang, L., Golts, A., Khapun, D., Shats, D., *et al.*: The kits21 challenge: Automatic segmentation of kidneys, renal tumors, and renal cysts in corticomedullary-phase ct. *arXiv preprint arXiv:2307.01984* (2023)
- [93] Ma, J., Zhang, Y., Gu, S., Zhu, C., Ge, C., Zhang, Y., An, X., Wang, C., Wang, Q., Liu, X., Cao, S., Zhang, Q., Liu, S., Wang, Y., Li, Y., He, J., Yang, X.: Abdomenct-1k: Is abdominal organ segmentation a solved problem? *IEEE Transactions on Pattern Analysis and Machine Intelligence* **44**(10), 6695–6714 (2022) <https://doi.org/10.1109/TPAMI.2021.3100536>
- [94] Armato III, S.G., McLennan, G., Bidaut, L., McNitt-Gray, M.F., Meyer, C.R., Reeves, A.P., Zhao, B., Aberle, D.R., Henschke, C.I., Hoffman, E.A., *et al.*: The lung image database consortium (lidc) and image database resource initiative (idri): a completed reference database of lung nodules on ct scans. *Medical physics* **38**(2), 915–931 (2011)
- [95] Nan, Y., Del Ser, J., Tang, Z., Tang, P., Xing, X., Fang, Y., Herrera, F., Pedrycz, W., Walsh, S., Yang, G.: Fuzzy attention neural network to tackle discontinuity in airway segmentation. *IEEE Transactions on Neural Networks and Learning Systems* (2023)

- [96] Roth, H.R., Xu, Z., Tor-Díez, C., Jacob, R.S., Zember, J., Molto, J., Li, W., Xu, S., Turkbey, B., Turkbey, E., *et al.*: Rapid artificial intelligence solutions in a pandemic—the covid-19-20 lung ct lesion segmentation challenge. *Medical Image Analysis* **82**, 102605 (2022)
- [97] Radl, L., Jin, Y., Pepe, A., Li, J., Gsaxner, C., Zhao, F.-h., Egger, J.: Avt: Multicenter aortic vessel tree cta dataset collection with ground truth segmentation masks. *Data in brief* **40**, 107801 (2022)
- [98] Kavur, A.E., Gezer, N.S., Barış, M., Aslan, S., Conze, P.-H., Groza, V., Pham, D.D., Chatterjee, S., Ernst, P., Özkan, S., Baydar, B., Lachinov, D., Han, S., Pauli, J., Isensee, F., Perkonnig, M., Sathish, R., Rajan, R., Sheet, D., Dovletov, G., Speck, O., Nürnberger, A., Maier-Hein, K.H., Bozdağı Akar, G., Ünal, G., Dicle, O., Selver, M.A.: CHAOS Challenge - combined (CT-MR) healthy abdominal organ segmentation. *Medical Image Analysis* **69**, 101950 (2021) <https://doi.org/10.1016/j.media.2020.101950>
- [99] Soler, L., Hostettler, A., Agnus, V., Charnoz, A., Fasquel, J.-B., Moreau, J., Osswald, A.-B., Bouhadjar, M., Marescaux, J.: 3d image reconstruction for comparison of algorithm database. URL: <https://www.ircad.fr/research/datasets/liver-segmentation-3d-ircadb-01> (2010)
- [100] Ginneken, B.: SLIVER07 [Data set]. Zenodo (2019). <https://doi.org/10.5281/zenodo.2597908> . <https://doi.org/10.5281/zenodo.2597908>
- [101] Morshid, A., Elsayes, K.M., Khalaf, A.M., Elmohr, M.M., Yu, J., Kaseb, A.O., Hassan, M., Mahvash, A., Wang, Z., Hazle, J.D., *et al.*: A machine learning model to predict hepatocellular carcinoma response to transcatheter arterial chemoembolization. *Radiology: Artificial Intelligence* **1**(5), 180021 (2019)
- [102] Roth, H.R., Farag, A., Turkbey, E.B., Lu, L., Liu, J., Summers, R.M.: Data From Pancreas-CT. <https://doi.org/10.7937/K9/TCIA.2016.tNB1kqBU>. The Cancer Imaging Archive (2016)
- [103] Žukovec, M., Dular, L., Špiclin, Ž.: Modeling multi-annotator uncertainty as multi-class segmentation problem. In: *International MICCAI Brainlesion Workshop*, pp. 112–123 (2021). Springer
- [104] Aerts, H.J., Velazquez, E.R., Leijenaar, R.T., Parmar, C., Grossmann, P., Carvalho, S., Bussink, J., Monshouwer, R., Haibe-Kains, B., Rietveld, D., *et al.*: Decoding tumour phenotype by noninvasive imaging using a quantitative radiomics approach. *Nature Communications* **5**(1), 4006 (2014)
- [105] Alves, N., *et al.*: The PANORAMA Study Protocol: Pancreatic Cancer Diagnosis-Radiologists Meet AI. Zenodo (2024). <https://doi.org/10.5281/zenodo.10599559> . <https://doi.org/10.5281/zenodo.10599559>

- [106] Qu, C., Zhang, T., Qiao, H., Tang, Y., Yuille, A.L., Zhou, Z., et al.: Abdomenatlas-8k: Annotating 8,000 ct volumes for multi-organ segmentation in three weeks. *Advances in Neural Information Processing Systems* **36** (2023)
- [107] Bassi, P.R., Li, W., Tang, Y., Isensee, F., Wang, Z., Chen, J., Chou, Y.-C., Kirchoff, Y., Rokuss, M.R., Huang, Z., et al.: Touchstone benchmark: Are we on the right way for evaluating ai algorithms for medical segmentation? *Advances in Neural Information Processing Systems* **37**, 15184–15201 (2024)
- [108] Buda, M., Saha, A., Mazurowski, M.A.: Association of genomic subtypes of lower-grade gliomas with shape features automatically extracted by a deep learning algorithm. *Computers in Biology and Medicine* **109**, 218–225 (2019)
- [109] Bernard, O., Lalande, A., Zotti, C., Cervenansky, F., Yang, X., Heng, P.-A., Cetin, I., Lekadir, K., Camara, O., Ballester, M.A.G., et al.: Deep learning techniques for automatic mri cardiac multi-structures segmentation and diagnosis: is the problem solved? *IEEE Transactions on Medical Imaging* **37**(11), 2514–2525 (2018)
- [110] Menze, B.H., Jakab, A., Bauer, S., Kalpathy-Cramer, J., Farahani, K., Kirby, J., Burren, Y., Porz, N., Slotboom, J., Wiest, R., et al.: The multimodal brain tumor image segmentation benchmark (brats). *IEEE Transactions on Medical Imaging* **34**(10), 1993–2024 (2014)
- [111] Gatidis, S., Hepp, T., Früh, M., La Fougère, C., Nikolaou, K., Pfannenberger, C., Schölkopf, B., Küstner, T., Cyran, C., Rubin, D.: A whole-body fdg-pet/ct dataset with manually annotated tumor lesions. *Scientific Data* **9**(1), 601 (2022)
- [112] Wang, X., Peng, Y., Lu, L., Lu, Z., Bagheri, M., Summers, R.M.: Chestx-ray8: Hospital-scale chest x-ray database and benchmarks on weakly-supervised classification and localization of common thorax diseases. In: *Proceedings of the IEEE Conference on Computer Vision and Pattern Recognition*, pp. 2097–2106 (2017)
- [113] Akbarnejad, A., Ray, N., Barnes, P.J., Bigras, G.: Predicting ki67, er, pr, and her2 statuses from h&e-stained breast cancer images. *arXiv preprint arXiv:2308.01982* (2023)
- [114] Kather, J.N., Halama, N., Marx, A.: 100000 Histological Images of Human Colorectal Cancer and Healthy Tissue. <https://doi.org/10.5281/zenodo.1214456> . <https://doi.org/10.5281/zenodo.1214456>
- [115] Tsuneki, M., Kanavati, F.: Inference of captions from histopathological patches. In: *International Conference on Medical Imaging with Deep Learning*, pp. 1235–1250 (2022). PMLR
- [116] He, X., Zhang, Y., Mou, L., Xing, E., Xie, P.: Pathvqa: 30000+ questions for

- medical visual question answering. arXiv preprint arXiv:2003.10286 (2020)
- [117] Kawai, M., Ota, N., Yamaoka, S.: Large-scale pretraining on pathological images for fine-tuning of small pathological benchmarks. In: Workshop on Medical Image Learning with Limited and Noisy Data, pp. 257–267 (2023). Springer
 - [118] Yan, K., Wang, X., Lu, L., Summers, R.M.: Deeplesion: automated mining of large-scale lesion annotations and universal lesion detection with deep learning. *Journal of medical imaging* **5**(3), 036501–036501 (2018)
 - [119] Lou, M., Ying, H., Liu, X., Zhou, H.-Y., Zhang, Y., Yu, Y.: Sdr-former: A siamese dual-resolution transformer for liver lesion classification using 3d multi-phase imaging. *Neural Networks*, 107228 (2025)
 - [120] Garrucho, L., Reidel, C.-A., Kushibar, K., Joshi, S., Osuala, R., Tsirikoglou, A., Bobowicz, M., Riego, J., Catanese, A., Gwoździwicz, K., et al.: Mama-mia: A large-scale multi-center breast cancer dce-mri benchmark dataset with expert segmentations. arXiv preprint arXiv:2406.13844 (2024)
 - [121] Lau, J.J., Gayen, S., Ben Abacha, A., Demner-Fushman, D.: A dataset of clinically generated visual questions and answers about radiology images. *Scientific data* **5**(1), 1–10 (2018)
 - [122] Liu, B., Zhan, L.-M., Xu, L., Ma, L., Yang, Y., Wu, X.-M.: Slake: A semantically-labeled knowledge-enhanced dataset for medical visual question answering. In: 2021 IEEE 18th International Symposium on Biomedical Imaging (ISBI), pp. 1650–1654 (2021). IEEE
 - [123] Lin, W., Zhao, Z., Zhang, X., Wu, C., Zhang, Y., Wang, Y., Xie, W.: Pmc-clip: Contrastive language-image pre-training using biomedical documents. In: International Conference on Medical Image Computing and Computer-Assisted Intervention, pp. 525–536 (2023). Springer
 - [124] Zhang, X., Wu, C., Zhao, Z., Lin, W., Zhang, Y., Wang, Y., Xie, W.: Pmc-vqa: Visual instruction tuning for medical visual question answering. arXiv preprint arXiv:2305.10415 (2023)
 - [125] Ye, J., Cheng, J., Chen, J., Deng, Z., Li, T., Wang, H., Su, Y., Huang, Z., Chen, J., Jiang, L., et al.: Sa-med2d-20m dataset: Segment anything in 2d medical imaging with 20 million masks. arXiv preprint arXiv:2311.11969 (2023)

Appendix A Extended Data

Table A1: Comparison of different representative biomedical models. Compared with previous methods, UniBiomed supports various modalities, prompts, and tasks. *LLM* denotes Large-Language Models. *Region-Aware Diagnosis* denotes models that can interpret regions of interest defined by users via visual prompts. *Pixel-level Grounding* indicates models that can generate text descriptions with corresponding segmentation masks. *End-to-End Training* indicates the models are trained in an end-to-end process.

Method	Multi-Modal	Support Prompts		Support Response			LLM	Region-Aware	Pixel-level	End-End
	Images	Visual	Text	Mask	Text	Mask+Text		Diagnosis	Grounding	Training
MedSAM [16]	✓	✓	✗	✓	✗	✗	✗	✗	✗	✓
BiomedParse [4]	✓	✗	✓	✓	✗	✗	✗	✗	✗	✓
3DSAM [65]	✗	✓	✗	✓	✗	✗	✗	✗	✗	✗
SegVol [23]	✗	✓	✗	✓	✗	✗	✗	✗	✗	✓
SAT [24]	✗	✗	✓	✓	✗	✗	✗	✗	✗	✓
MedSAM2 [57]	✓	✓	✗	✓	✗	✗	✗	✗	✗	✓
M3D [42]	✗	✗	✓	✓	✓	✗	✓	✗	✗	✗
RadFM [47]	✗	✗	✓	✗	✓	✗	✓	✗	✗	✗
LLaVA-Med [12]	✓	✗	✓	✗	✓	✗	✓	✗	✗	✗
BiomedGPT [8]	✓	✗	✓	✗	✓	✗	✓	✗	✗	✓
fVLM [48]	✗	✗	✓	✗	✓	✗	✗	✓	✗	✓
MedRegA [13]	✓	✓	✓	✗	✓	✗	✓	✓	✗	✓
MedPLIB [14]	✓	✓	✓	✓	✓	✗	✓	✓	✓	✗
UniBiomed	✓	✓	✓	✓	✓	✓	✓	✓	✓	✓

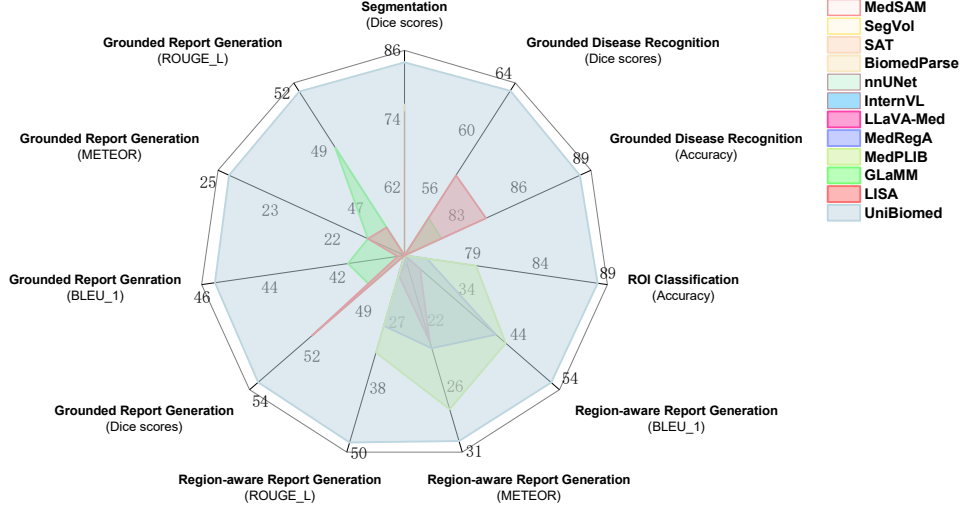


Fig. A1: Overall comparisons on various biomedical tasks, including segmentation, disease recognition, ROI classification, region-aware report generation, and grounded report generation. We compare UniBiomed with MedSAM [16], BiomedParse [4], SegVol [23], SAT [24], InternVL2.5 [26], LLaVA-Med [12], MedRegA [13], MedPLIB [14], GLaMM [41], and LISA [31]. Notably, while previous methods can address only a limited number of these tasks, UniBiomed excels by delivering state-of-the-art performance across all of them.

Table A2: 61 datasets across 10 modalities for segmentation, ROI classification, and grounded disease recognition. 47 and 14 of them are used for internal and external validation, respectively. The external datasets are annotated with *.

Dataset	Modality	Link
CXRMask [66]	X-Ray	https://datasetninja.com/chest-xray
Radiography [67]	X-Ray	https://www.kaggle.com/datasets/tawafurrahman/covid19-radiography-database
COVID-QU-Ex [68]	X-Ray	https://www.kaggle.com/datasets/anasmohammedtahir/covidqu
CDD-CESM [69]	X-Ray	https://www.cancerimagingarchive.net/collection/cdd-cesm/
SIIM [70]	X-Ray	https://www.kaggle.com/datasets/vbookshelf/pneumothorax-chest-xray-images-and-masks
PanNuke [71]	Pathology	https://jgamper.github.io/PanNukeDataset/
GlaS [72]	Pathology	https://warwick.ac.uk/fac/cross_fac/tia/data/glascontest/
CoCaHis [73]	Pathology	https://cocahis.irb.hr/
CryoNuSeg [74]	Pathology	https://github.com/masih4/CryoNuSeg
DigestPath [75]	Pathology	https://digestpath2019.grand-challenge.org/
SICAPv2 [76]	Pathology	https://data.mendeley.com/datasets/9xxm58dvs3/1
WSSS4LUAD [77]	Pathology	https://wss4luad.grand-challenge.org/
CRAG* [78]	Pathology	https://warwick.ac.uk/fac/cross_fac/tia/data/mildnet/
MoNuSeg* [79]	Pathology	https://monuseg.grand-challenge.org/
US [80–82]	Ultrasound	https://www.kaggle.com/datasets/ignaciolarlando/ussimandsegm
REFUGE [83]	Fundus	https://bitbucket.org/woaldnd/refuge/src
DRIVE [84]	Fundus	https://drive.grand-challenge.org/
UWater [85]	Dermoscopy	https://uwaterloo.ca/
NeoPolyp [86]	Endoscope	https://www.kaggle.com/c/bkai-igh-neopolyp/data
OCT-CME [87]	OCT	https://www.kaggle.com/datasets/zeeshanahmed13/intraretinal-cystoid-fluid
MSD [7]	CT&MRI	http://medicaldecathlon.com/
AMOS [88]	CT&MRI	https://amos22.grand-challenge.org/
BTCV [89]	CT	https://www.synapse.org/#!Synapse:syn3193805/wiki
WORD [90]	CT	https://github.com/HILab-git/WORD
FLARE22 [91]	CT	https://flare22.grand-challenge.org/
FLARE23* [91]	CT	https://codalab.lisn.upsaclay.fr/competitions/12239
KiTS23 [92]	CT	https://kits-challenge.org/kits23/
AbdomenCT1K* [93]	CT	https://github.com/JunMa11/AbdomenCT-1K
LIDC-IDRI [94]	CT	https://www.cancerimagingarchive.net/collection/lidc-idri/
AIIB [95]	CT	https://codalab.lisn.upsaclay.fr/competitions/13238
COVID-CT [96]	CT	https://covid-segmentation.grand-challenge.org/
AVT [97]	CT	https://figshare.com/articles/dataset/Aortic_Vessel_Tree_AVT_CTA_Datasets_and_Segmentations/
CHAOS* [98]	CT	https://chaos.grand-challenge.org/
IRCAdb* [99]	CT	https://www.ircad.fr/research/data-sets/liver-segmentation-3d-ircadb-01
SLIVER07* [100]	CT	https://sliver07.grand-challenge.org/
HCCTACE* [101]	CT	https://www.cancerimagingarchive.net/collection/hcc-tace-seg
TCIAPancreas* [102]	CT	https://www.cancerimagingarchive.net/collection/pancreas-ct/
QUBIQ* [103]	CT	https://qubiq21.grand-challenge.org/QUBIQ/
Rider* [104]	CT	https://www.cancerimagingarchive.net/analysis-result/rider-lungct-seg/
PANORAMA* [105]	CT	https://panorama.grand-challenge.org/
AbdomenAtlas* [106, 107]	CT	https://github.com/MrGiovanni/AbdomenAtlas
RadGenome [43]	CT	https://huggingface.co/datasets/RadGenome/RadGenome-ChestCT
LGG [108]	MRI	https://www.kaggle.com/datasets/mateuszbudala/lgg-mri-segmentation
ACDC [109]	MRI	https://www.creatis.insa-lyon.fr/Challenge/acdc/databases.html
BraTS21* [110]	MRI	https://www.synapse.org/Synapse:syn51156910/wiki/621282
AutoPET [111]	PET	https://autopet.grand-challenge.org/

Table A3: 23 Datasets across 10 modalities for training and validation of report generation. Multi-modal contains: X-ray, Pathology, Endoscopy, Ultrasound, Dermoscopy, Fundus, PET, CT, OCT, and MRI. The bounding box annotations are generated by MedTrinity [15].

Dataset	Modality	Link
NIH-CXR [112]	X-Ray	https://www.kaggle.com/datasets/nih-chest-xrays/data
Breast Histopathology	Pathology	https://www.kaggle.com/datasets/paultimothymooney/breast-histopathology-images
BreastCancer	Pathology	https://zenodo.org/records/6633721
CISC	Pathology	https://academictorrents.com/details/99f2c7b57b95500711e33f2ee4d14c9fd7c7366c
CPD	Pathology	https://zenodo.org/records/7282326
IHC4BC [113]	Pathology	https://www.kaggle.com/datasets/akbarnejad1991/ihc4bc-compressed/data
NCT-CRC-HE-100K [114]	Pathology	https://www.kaggle.com/datasets/imrankhan77/nct-crc-he-100k
PatchGastricADC22 [115]	Pathology	https://zenodo.org/records/6550925
Path-VQA [116]	Pathology	https://huggingface.co/datasets/flaviagammarino/path-vqa
TCGA-UT	Pathology	https://zenodo.org/records/5889558
PTCGA [117]	Pathology	https://drive.google.com/drive/folders/18CmL-WLyppK1Rk29CgV7ib5MACFzg5ei
BHX	CT	https://physionet.org/content/bhx-brain-bounding-box/1.1/
DeepLesion [118]	CT	https://huggingface.co/datasets/farrell236/DeepLesion
CT-RATE [29]	CT	https://huggingface.co/datasets/ibrahimhamamci/CT-RATE
RadGenome [43]	CT	https://huggingface.co/datasets/RadGenome/RadGenome-ChestCT
BRATS24-MICCAI	MRI	https://www.synapse.org/Synapse:syn53708126
LLD-MMRI [119]	MRI	https://github.com/LMMMEng/LLD-MMRI-Dataset
MAMA-MIA [120]	MRI	https://www.synapse.org/Synapse:syn60868042/wiki/628716
VQA-RAD [121]	X-Ray&MRI	https://osf.io/89kps/
SLAKE [122]	X-Ray&CT&MRI	https://www.med-vqa.com/slake/
PMC-OA [123]	Multi-modal	https://huggingface.co/datasets/axiong/pmc_oa
PMC-VQA [124]	Multi-modal	https://huggingface.co/datasets/xmcnic/PMC-VQA
SA-Med2D-20M [125]	Multi-modal	https://openxlab.org.cn/datasets/GMAI/SA-Med2D-20M

Table A4: Descriptions of datasets used in this work. We present the modalities, regions of interest, and number of triplets (image-text-annotation) in the table.

Dataset	Modality	Regions of interest	Number of triplets
CXRMask [66]	X-Ray	Chest	1,698
Radiography-Lung-opacity [67]	X-Ray	chest	6,012
Radiography-Normal [67]	X-Ray	chest	30,574
Radiography-Viral-Pneumonia [67]	X-Ray	chest	1,345
COVID-QU-Ex [68]	X-Ray	Chest & COVID19 infection	20,385
CDD-CESM [69]	X-Ray	Breast lesion	1,233
SIIM [70]	X-Ray	Pneumothorax	2,669
PanNuke [71]	Pathology	Connective tissue, inflammatory, neoplastic, and dead cells	32,450
GlaS [72]	Pathology	Gland tissue	330
CoCaHis [73]	Pathology	Colon cancer	82
CryoNuSeg [74]	Pathology	Nuclei	30
DigestPath [75]	Pathology	Malignant lesion in colon tissue	13,391
SICAPv2 [76]	Pathology	Prostate cancer	23,924
WSSS4LUAD [77]	Pathology	Lung tumor	5,735
CRAG [78]	Pathology	Gland tissue	1,750
MoNuSeg [79]	Pathology	Nuclei	51
BreastUS [80]	Ultrasound	Breast lesion	1,294
LiverUS [80]	Ultrasound	Liver	39
CAMUS [81]	Ultrasound	Heart	42,463
FH-PS-AOP [82]	Ultrasound	Transperineal	8,000
REFUGE [83]	Fundus	Retinal	2,400
DRIVE [84]	Fundus	Retinal	20
UWater [85]	Dermoscopy	Skin lesion	325
NeoPolyp [86]	Endoscope	Colon polyp	2,050
OCT-CME [87]	OCT	Retinal edema	1,460
BTCV [89]	CT	Abdomen organs	12,176
AMOS22 [88]	CT	Abdomen organs	138,371
WORD [90]	CT	Abdomen organs	58,898
FLARE22 [91]	CT	Abdomen organs	26,802
FLARE23 [91]	CT	Abdomen organs	4,760,889
Abdomenct1k [93]	CT	Abdomen organs	1,006,170
AbdomenAtlas [106]	CT	Abdomen organs	3,722,697
AVT [97]	CT	Aorta	4,988
CHAOS [98]	CT	Liver	2,341
Sliver07 [100]	CT	Liver	2,750
IRCADb [99]	CT	Liver & Liver Tumor	3,420
HCCTACE [99]	CT	Liver & Liver Tumor	9,947
KITS [92]	CT	Kidney & Kidney Tumor	44,557
TCIAPancreas [102]	CT	Pancreas	6,882
PANORAMA [105]	CT	Pancreas & Pancreas Tumor	477,437
QUBIQ [103]	CT	Pancreas & Pancreas Tumor	809
LIDC-IDRI [94]	CT	Lung nodule	9,122
COVID-CT [96]	CT	COVID	1,572
RIDER [104]	CT	Lung Tumor	1,484
AIIB23 [95]	CT	Fibrotic Lung disease	51,715
MSD03 Liver [7]	CT	Liver & Liver Tumor	21,810
MSD06 Lung [7]	CT	Lung Tumor	1,483
MSD07 Panc. [7]	CT	Pancreas & Pancreas Tumor	10,695
MSD08 Vessel [7]	CT	Liver Vessel Tumor	13,201
MSD09 Spleen [7]	CT	Spleen	982
MSD10 Colon [7]	CT	Colon Tumor	1,245
RadGenome [29, 43]	CT	Abdomen&Chest	81,257
AMOS-MRI [88]	MRI	Abdomen	52,625
ACDC [109]	MRI	Heart	7,666
LGG [108]	MRI	Brain Tumor	2,542
MSD01 Brain [7]	MRI	Brain Tumor	380,720
MSD02 Heart [7]	MRI	Heart	1,207
MSD04 Hip. [7]	MRI	Hippocampus	7,770
MSD05 Pros. [7]	MRI	Prostate	1,434
MedTrinity [15]	Multi-modal	Whole body	16,270,486
Total			27,408,704

Table A5: Number of images and image-text-annotation triplets across different imaging modalities. Specifically, an image may contain numerous regions of interest, and each region of interest is paired with text descriptions and localization annotations (segmentation masks or bounding boxes).

Modality	Number of images	Number of triplets
X-Ray	79,212	122,613
Pathology	4,029,165	4,056,746
CT	8,171,448	16,193,612
MRI	6,630,101	6,956,286
Ultrasound	26,066	51,944
Fundus	1,436	2,636
Dermoscopy	6,616	6,735
Endoscope	4,061	5,111
OCT	1,484	1,484
PET	11,561	11,561
Total	18,961,150	27,408,704

Table A6: 270K images with 15 types of abnormalities for grounded disease recognition experiments. 66,226 normal images as negative samples are also included in training and validation, constructing a dataset of 341,284 images. We split the datasets into 80% training and 20% test sets. The links to the datasets are provided in Table A2.

Abnormality	Number	Datasets
Liver tumor	10,338	MSD03-Liver [7]
Pancreas tumor	2,504	MSD07-Pancreas [7]
Kidney tumor	12,182	KiTS23 [92]
Colon cancer	14,718	MSD10-Colon [7], CoCaHis [73], DigestPath [75]
Lung tumor	1,483	MSD06-Lung [7]
Lung nodule	9,122	LIDC [94]
COVID19 infection	21,957	COVID-QU-Ex [68], COVID-CT [96]
Fibrotic lung disease	51,715	AIIB [95]
Brain tumor	119,523	LGG [108], MSD01-Brain [7]
Breast lesion	1,294	BreastUS [80]
Colon polyp	2,050	NeoPolyp [86]
Pneumothorax	2,669	Pneumonia [67]
Prostate cancer	23,924	SICAPv2 [76]
Skin lesion	119	UWater [85]
Retinal lesion	1,460	OCT-CME [87]
No findings	66,226	CXRMask [66], CAMUS [81], FH-PS-AOP [82] MSD [7], CHAOS [98], KiTS23 [92]
Total	341,284	

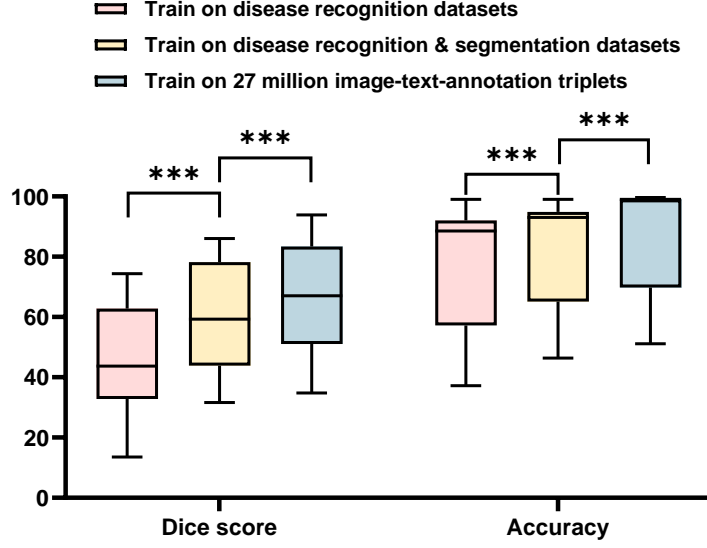


Fig. A2: Ablation studies of grounded disease recognition. We conduct ablation studies to demonstrate that universal training on different types of datasets can effectively improve the Dice scores and accuracy of grounded disease recognition. We evaluate the effectiveness of training datasets: (1) only train on disease recognition datasets (**Extended Data Table A6**); (2) add segmentation datasets for segmentation training; (3) train on the whole 27 million triplet dataset. Specifically, segmentation training improves dice scores by 20.32% ($***P < 1 \times 10^{-3}$) and accuracy by 4.90% ($***P < 1 \times 10^{-3}$), respectively. Universal training on 27 million triplets improves dice scores by 7.15% ($***P < 1 \times 10^{-3}$) and accuracy by 4.37% ($***P < 1 \times 10^{-3}$), respectively. These findings robustly validate the effectiveness of universal training in improving grounded biomedical image interpretation.

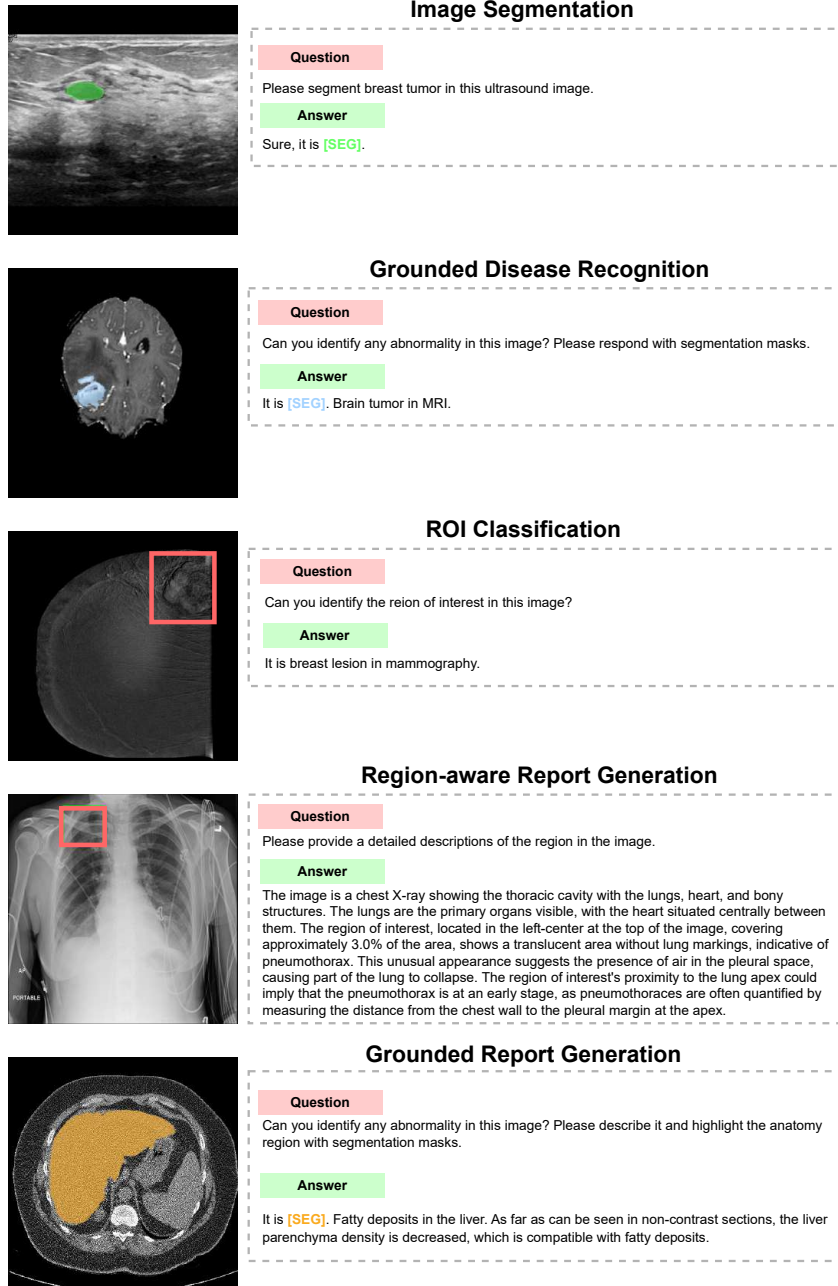


Fig. A3: Uniform VQA format for universal training. For different biomedical tasks, we process the datasets into the same format as above. We present the data format for image segmentation, disease recognition, ROI classification, region-aware report generation, and grounded report generation.

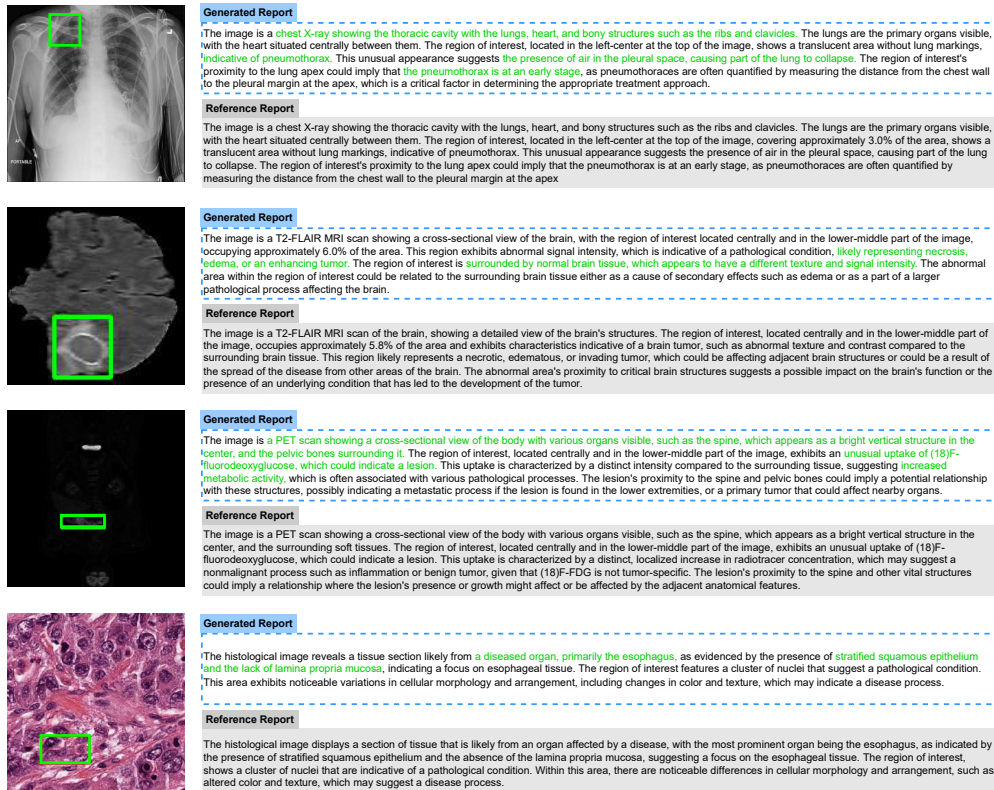


Fig. A4: Region-aware report generation results on the MedTrinity [15] dataset. The text in green indicates the correct contents in generated reports.

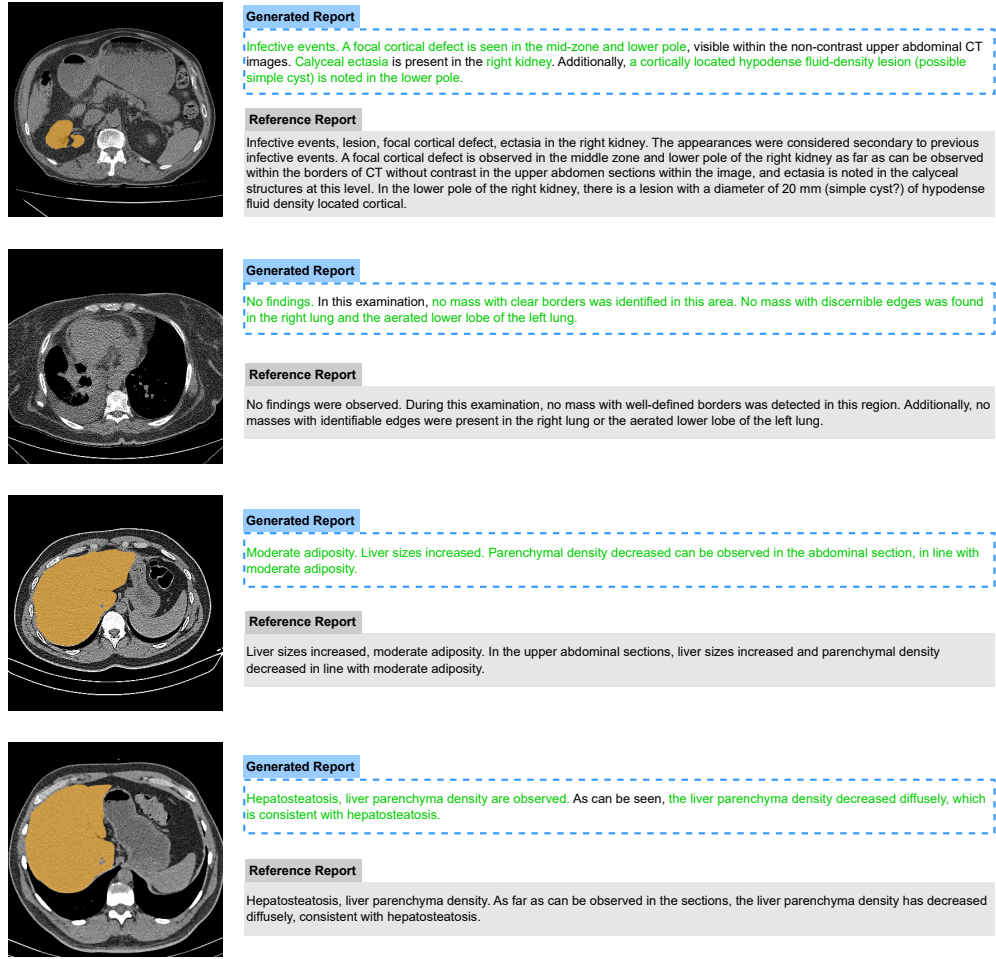


Fig. A5: Grounded report generation results on the RadGenome [43] dataset. The generated segmentation masks are in orange, which indicate the location of the corresponding organs described in the reports. The text in green indicates the correct contents in generated reports.

Table A7: The public codes of methods used in this study.

Method	Sources
SAM2 [28]	https://github.com/facebookresearch/sam2
InternVL [26]	https://github.com/OpenGVLab/InternVL
SA2VA [30]	https://github.com/magic-research/Sa2VA
LISA [31]	https://github.com/dvlab-research/LISA
GLaMM [41]	https://github.com/mbzuai-oryx/groundingLMM
Osprey [44]	https://github.com/CircleRadon/Osprey
VoCo [62, 63]	https://github.com/Luffy03/Large-Scale-Medical
MedSAM [16]	https://github.com/bowang-lab/MedSAM
BiomedParse [4]	https://github.com/microsoft/BiomedParse
SegVol [23]	https://github.com/BAAI-DCAI/SegVol
SAT [24]	https://github.com/zhaoziheng/SAT
LLaVA-Med [12]	https://github.com/microsoft/LLaVA-Med
MedRegA [13]	https://github.com/xmed-lab/MedRegA
MedPLIB [14]	https://github.com/ShawnHuang497/MedPLIB
MedTrinity [15]	https://github.com/UCSC-VLAA/MedTrinity-25M

Table A8: Architecture details and Training settings.

MLLM	InternVL2.5
Segmentation Model	SAM2-hiera-large
Network Params	1.23 B
Segmentation Loss	Dice+Cross Entropy
LLM Loss	Cross Entropy
Platform	Pytorch 2.3.1
CUDA version	11.8
Training GPU(s)	8*NVIDIA H800 (80G)
Inference GPU(s)	1*NVIDIA 3090 (24G)
Training epochs	10
Training time	120 hours
Batch size	32
Optimizer	AdamW
Scheduler	Warmup+Cosine
Learning rate	4e-5
Image size	1024 \times 1024
Inference time	Average 0.175 s/image